Linköping Studies in Science and Technology
Licentiate Thesis No. 1799

Oxidation behaviour of MCrAlX coatings: effect of surface treatment and an Al-activity based life criterion

Pimin Zhang

张丕敏

Division of Engineering Materials
Departement of Management and Engineering (IEI)
Linköping University, SE-581 83 Linköping, Sweden

Linköping 2018

Front page images: (1) low magnification of snowflake like α-Al_2O_3 formed on polished coating surface after 10 h oxidation; (2) blade-like transient Al_2O_3 formed on shot-peened coating surface after 100 min oxidation; (3) spinel island formed on polished coating surface after 10 min oxidation.
Cover page: designed by Wanjun Chu.

During the course of research underlying this thesis, Pimin Zhang was enrolled in Agora Materiae, a multidiciplinary doctoral program at Linköping University, Sweden.

ISBN 978-91-7685-381-8
ISSN 0280-7971

Printed by LiU-Tryck 2018

Abstract

MCrAlY coatings (M=Ni and/or Co) have been widely used for the protection of superalloy components against oxidation and hot corrosion in the hot sections of gas turbines. The drive to improve engine combustion efficiency while reducing emissions by increasing the operation temperature brings a big challenge for coating design. As a result, the need for improvement of MCrAlY coatings for better oxidation resistance is essential.

Formation of a stable, dense, continuous, and slow-growing α-Al_2O_3 layer, on the MCrAlY coating surface, is the key to oxidation protection, since the protective α-Al_2O_3 scale offers superior oxidation resistance due to its lower oxygen-diffusion rate as compared with other oxides. The ability of a MCrAlY coating to form and maintain such a protective scale depends on the coating composition and microstructure, and can be improved through optimization of deposition parameters, modification of coating surface conditions, and so on. Part of this thesis work focuses on studying the effect of post-deposition surface treatments on the oxidation behavior of MCrAlX coatings (X can be yttrium and/or other minor alloying elements). The aim is to gain fundamental understanding of alumina scale evolution during oxidation which is important for achieving improved oxidation resistance of MCrAlX coatings. Oxide scale formed on coatings at initial oxidation stage and the effect of surface treatment were investigated by a multi-approach study combining photo-stimulated luminescence, microstructural observation and weight gain. Results showed that both mechanically polished and shot-peened coatings exhib-

ited superior performance due to rapid formation of α-Al_2O_3 fully covering the coating and suppressing growth of transient alumina, assisted by the high density of α-Al_2O_3 nuclei on surface treatment induced defects. The early development of a two-layer alumina scale, consisting of an inward-grown inner α-Al_2O_3 layer and an outer layer transformed from outward-grown transient alumina, resulted in a higher oxide growth rate of the as-sprayed coating. The positive effect of the surface treatments on retarding oxide scale growth and suppressing formation of spinel was also observed in oxidation test up to 1000 hrs.

As the oxidation proceeds to the close-to-end stage, a reliable criterion to estimate the capability of coating to form α-Al_2O_3 is of great importance to accurately evaluate coating lifetime, which is the aim of the other part of the thesis work. Survey of published results on a number of binary Ni-Al and ternary Ni-Cr-Al, Ni-Al-Si systems shows that the empirical Al-concentration based criterion is inadequate to properly predict the formation of a continuous α-Al_2O_3 scale. On the other hand, correlating the corresponding Al-activity data, calculated from measured chemical compositions using the Thermo-Calc software, to the experimental oxidation results has revealed a temperature dependent, critical Al-activity value for forming continuous α-Al_2O_3 scale. To validate the criterion, long-term oxidation tests were performed on five MCrAlX coatings with varying compositions and the implementation of the Al-activity based criterion on these coatings successfully predicted α-Al_2O_3 formation, showing a good agreement with experiment results.

Populärvetenskaplig sammanfattning

MCrAlY-ytbeläggningar (M=Ni och/eller/Co)) har i stor utsträckning använts för att skydda komponenter gjorda utav superlegeringar, mot oxidation och korrosion vid hög temperatur i de heta delarna av gasturbiner. Drivkraften att genom ökad driftstemperatur förbättra förbränningseffektiviteten i gasturbiner samtidigt som utsläppen minskas, innebär en stor utmaning vid utveckling av nya ytbeläggningar. Som ett resultat av detta är behovet av förbättrade MCrAlY-ytbeläggningar med bättre oxidationsmotstånd av stor betydelse.

Nyckeln till ett bra oxidationsskydd är bildandet av ett stabilt, tätt, kontinuerligt samt långsamt växande α-Al_2O_3-skikt vid MCrAlY-ytbeläggningens yta. Detta eftersom det skyddande α-Al_2O_3-skiktet ger ett överlägset oxidationsskydd tack vare en lägre diffusionshastighet av syre jämfört med andra oxidskikt. Förmågan hos en MCrAlY-ytbeläggning att bilda och bibehålla ett sådant skyddande oxidskikt beror på ytbeläggningens kemiska komposition och dess mikrostruktur. Det dessutom kan förbättras genom optimering av sprutningssparametrar, modifiering av ytbeläggningsytor osv. En del av denna avhandling fokuserar på effekten av ytbehandling metoder på oxidationsbeteendet hos MCrAlX-ytbeläggningar (X betecknar yttrium och/eller andra mindre legeringsämnen). Syftet är att erhålla en grundläggande förståelse för aluminiumoxidskiktets utveckling under oxidationsprocessen, vilket är betydelsefullt för att uppnå ett förbättrat oxidationsmotstånd hos MCrAlX-ytbeläggningar. Genom en studie som kombinerar fotostimulerad luminiscens, mikrostrukturundersökning samt viktökningsanalys kunde oxidskikten

som bildats vid det tidiga oxidationsstadiet och effekten av ytbehandlingar undersökas. Resultaten visade att både mekaniskt polerade och kulpenade ytbeläggningar påvisade överlägsen prestanda tack vare ett hastigt bildande av α-Al_2O_3 som fullständigt täckte ytbeläggningens yta samt undertrycker tillväxten av transient aluminiumoxid. Den högre oxidtillväxthastigheten hos den icke behandlade ytbeläggningen förklarades av tidigt utveckling av ett aluminiumoxidskikt med två lager, bestående av ett inåtväxande α-Al_2O_3 innerskikt och ett yttre skikt transformerat från en utåt växande transient aluminiumoxid på ytbeläggningens yta. Den positiva effekten av ytbehandlingar bekräftades också med en ytterligare studie av långtidsoxidation av MCrAlX-ytbeläggningar.

Då oxidationsprocessen är nära slutstadiet, blir det viktigt med ett tillförlitligt kriterium för bildandet av ett kontinuerligt α-Al_2O_3 skikt som kan användas för att ytbeläggningens livslängd noggrant ska kunna utvärderas. Att utveckla ett sådant kriterium är syftet med den andra delen av avhandlingen. En litteraturstudie av publicerade resultat på ett antal binära Ni-Al och ternära Ni-Cr-Al, Ni-Al-Si-system visar att det empiriska Al-koncentrationsbaserade kriteriet är otillräckligt för att korrekt förutsäga bildandet av ett kontinuerlig α-Al_2O_3-skikt. Å andra sidan har korrelation av motsvarande Al-aktivitetsdata, beräknad från uppmätta kemiska kompositioner med användning av Thermo-Calc-mjukvaran, och oxidationsresultaten visat ett temperaturberoende kritiskt Al-aktivitetsvärde för bildandet av ett kontinuerligt α-Al_2O_3-skikt. Kriteriet validerades i ett långsiktigt oxidationstest på fem MCrAlX ytbeläggningar och goda överenskommelser erhölls mellan det ytbeläggningslivet som beräknades från Al-aktiviteten och de experimentella resultaten.

Acknowledgements

The present project is financed by Siemens Industrial Turbomachinery AB, Swedish Energy Agency through KME consortium - ELFORSK, and are therefore grateful acknowledged. This project work has been carried out at Division of Engineering materials, Department of Management and Engineering, Linköping University, Sweden.

Firstly, I would like to express my sincere gratitude to my supervisor, Prof. Ru Lin Peng, not only for her infinite enthusiasm and support, but also for having an open-mind for my research interests. Through the valuable discussions and constructive comments, I have learned a lot on how to write a good scientific paper. Secondly, I want to thank my co-supervisor Dr.Xin-Hai Li, from Siemens Industrial Turbomachinery AB, for providing the valuable guidance and fruitful discussions. The practical industrial experiences often bring new aspects for the research. Also, the inputs from Prof. Sten Johansson and support on TMF testings from Prof. Johan Moverare are also greatly appreciated.

Special thanks are addressed to Kang Yuan, a former PhD from our division, who has done a great job in Phase I of this project: a good design of alloy composition and a well-constructed characterization procedure as a guidance for Phase II. My thanks also go to my collaborators from University West, Esmaeil Sadeghimeresht and Mohit Gupta, who have been quite efficient and productive for providing materials and inspiring discussions, to Prof. Shrikant Joshi and Prof. Nicolaie Markocsan for their valuable comments and supports on paper writing.

I would like to thank Shula Chen and Mattias Jansson from IFM for the support on PSLS measurement.

I also want to thank all my colleagues in Engineering Materials for their friendship, encouragement, discussion, and support during the study. I'd like to especially thank Krishna Praveen Jonnalagadda, whom I share office with, for the many constructive discussions and creating a productive environment, to Dunyong for being a good friend and gym buddy, and to Mattias Calmunger for translating the abstract to Swedish. A special thanks to Mrs. Ingmari Hallkvist for the best administrative support. I'm also grateful to my Chinese friends from physics department for having fun together and to Wanjun for the nice design of the cover page.

At last, I want to thank my parents for always being supportive, patient, and cheerful during the dark "snowy" days. Especially, the positive environment I was raised up to build a optimistic personality, the ability to stay positive at difficult times makes PhD life less stressful.

PIMIN (KYLE)

Linköping, January 2018

Contents

Abbreviations

BC	**B**ond **C**oat
BCC	**B**ody **C**entered **C**ubic
BLZ	β-**L**eft **Z**one
BSE	**B**ack**S**cattered **E**lectron
CTE	**C**oefficient of **T**hermal **E**xpension
EDS	**E**lectron **D**ispersive X-ray **S**pectroscopy
FCC	**F**ace **C**entered **C**ubic
GPDZ	**G**amma-**P**rime-**D**epletion **Z**one
HVAF	**H**igh **V**elocity **A**ir-**F**uel
HVOF	**H**igh **V**elocity **O**xygen-**F**uel
IBDZ	**I**nner-β-**D**epletion **Z**one
LSM	**L**aser **S**urface **M**elting
OBDZ	**O**uter-β-**D**epletion **Z**one
PSLS	**P**hoto-**S**timulated **L**uminesce **S**pectroscopy
RE	**R**eactive **E**lement
SE	**S**econdary **E**lectron
SEM	**S**canning **E**lectron **M**icroscopy

TBC	**T**hermal **B**arrier **C**oating
TC	**T**op **C**oat
TCP	**T**opologically **C**lose **P**acked
TGO	**T**hermally **G**rown **O**xide
WDS	**W**avelength **D**ispersive **S**pectroscopy
XRD	**X**-**R**ay **D**iffraction

List of Papers

The following papers have been included in this thesis:

Paper I

P. Zhang, K. Yuan, R. Lin Peng, X.-H. Li, S. Johansson. Long-term oxidation of MCrAlY coatings at 1000 ℃ and an Al-activity based coating life criterion. *Surface and Coating Technology*, 332C(2017) 12-21.

Paper II

P. Zhang, E. Sadeghimeresht, S. Chen, X.-H. Li, N. Markocsan, S. Joshi, W. Chen, I.A. Buyanova, R. Lin Peng. A multi-approach study of transient→alpha transformation in alumina scale formed on HVAF-sprayed NiCoCrAlY coatings and the effect of surface treatment. *Submitted to Corrosion Science*.

Paper III

P. Zhang, E. Sadeghimeresht, R. Lin Peng, X.-H. Li, N. Markocsan, S. Joshi, S. Johansson. Isothermal oxidation behavior of HVAF-sprayed NiCoCrAlY coatings: Effect of surface treatment. *Proceedings of International Thermal Sprayed Conference (ITSC)*, May 7-9, Germany, pp. 456-461, 2017.

Contribution to the papers included:

For above papers, I have been the main contributor of the characterization of materials and manuscript writing. In addition, Kang Yuan conducted oxidation tests in Paper I.

Paper not included in this thesis:

Paper IV

P. Zhang, R. Lin Peng, X.-H. Li, S. Johansson. Influence of Ce and Ru on the Behaviour of HVOF NiCoCrAlX Coatings in High Temperature Oxidation. *Proceedings of International Thermal Sprayed Conference (ITSC)*, May 10-12, China, pp. 635-640, 2016.

Part I

Background & Theory

CHAPTER 1

Introduction

1.1 Background

With the increasing of population and industrial development worldwide, the demand for electricity is expanding and will continue to grow. Among many energy resources to generate electricity, such as fossil fuel power plants, nuclear power plant and other renewable energy options, over 80 % of the electricity is derived from heat sources [1]. Although the proportion of energy generation of renewable energy options are increasing, more than 65 % of energy generation is still relied on the combustion of fossil fuel by turbines, like coal, oil and gas. It is reported that a high efficiency can be achieved by the modern fossil fuel power plant [1, 2]. Industrial gas turbine, since it has been firstly applied in power generation back to 1939, has been the most widely used to produce electricity from heat resources [3]. With the increasing demand of electricity, concerns about air pollution and CO_2 emissions induced by the fossil fuel combustion, it is urgent to improve the efficiency of gas turbines and reduce fuel consumption. The goal of industry is to improve fuel efficiency and reduce CO_2 emissions of gas turbines through a good gas turbine design and the development of durable materials which provide better performances at elevated temperature including superalloys and functional coating systems [3–6].

1.2 Gas turbines

Despite the different applications of gas turbine, such as power generation and aircraft propulsion, the overall design might vary but the operation principle remains the same, as illustrated in Fig. 1.1. During operation of the gas turbines, air is taken through the INTAKE and compressed by COMPRESSOR in order to increase the temperature of inlet gases. Then the compressed air is mixed with fuels when enters the COMBUSTOR chamber. By igniting the mixture, hot gases with high-temperature and high-pressure are produced, which impact the blades and vanes in the TURBINE section to drive the shaft to generate power. The gas flow achieves the highest temperature, ranging from 927-1593 ℃ [6], when passing through the first stage of TURBINE next to COMBUSTOR. Afterwards, the gases leave the gas turbine though the EXHAUST with pressure drop and temperature reduction. A gas turbine, such as SGT-800 as shown in Fig. 1.1, can achieve a high energy efficiency up to 40 % [7].

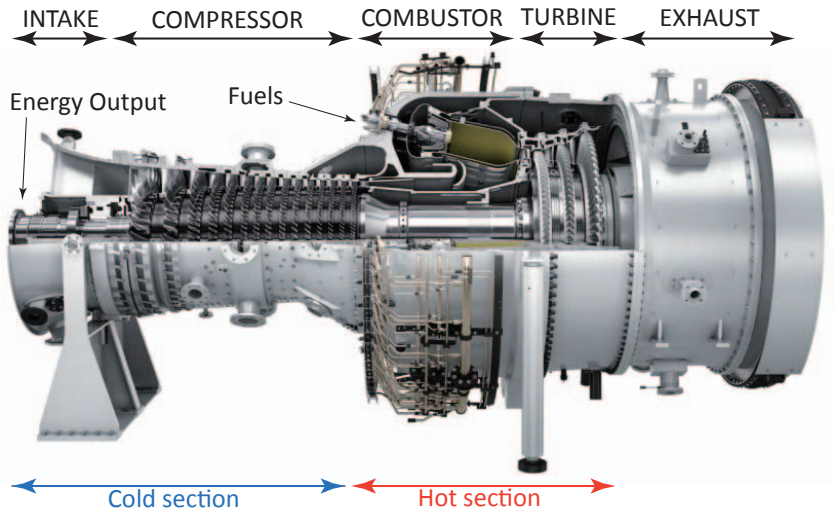

Figure 1.1. Section of stationary gas turbines SGT-800 from Siemens. Courtesy of Siemens

Considering service conditions in different sections of gas turbine, various materials are chosen based on their mechanical properties and the temperature limitation. As illustrated in Fig. 1.1, the INTAKE and COMPRESSOR generally maintain the temperature below 600 ℃, Fe-based alloys are therefore used to manufacture these parts. The temperature of gas increases dramatically in the

COMBUSTOR and TURBINE sections. Therefore, Ni- and Co-based superalloys are needed as the base materials for the blades and vanes in these sections sustained even up to about 1000 ℃ [3, 4]. Considering the severe operation condition of these sections, protective coatings are required to provide oxidation and hot corrosion resistance for superalloy-base components. The coatings used are usually alumina-former as the formation of protective dense and adhesive thermally grown alumina scale at coating/gas interface shield the components from the harsh working environment. In some parts of the gas turbine where the service temperature is even higher, thermal barrier coatings (TBCs) are used on the components to decrease the temperature of the metallic materials, cooperated an internal cooling systems in the metallic components [8].

1.3 Importance of MCrAlX coatings

MCrAlX (M: Ni and/or Co; X: minor elements) coatings have been largely used in hot component of gas turbine to provide protection against high temperature oxidation and hot corrosion for the base materials. MCrAlX coatings are utilized as overlay on blades in the end part of the COMBUSTOR, blades and vanes in the low-temperature part of the TURBINE; bond coats in TBC systems in the COMBUSTOR section and in high-temperature part of the TURBINE section. The reasons and benefits to use MCrAlX coatings in gas turbines can be summarized as follows:

- To provide protection for base materials from high-temperature oxidation and hot corrosion by forming a protective oxide scale on coating;
- Coating composition can be tailored to meet various application requirement;
- Coating thickness can easily be controlled according to the demands;
- Flexible coating deposition methods can be chosen from for different applications;
- A good combination of durability and mechanical properties, such as strength and ductility at high temperature, can be achieved;
- To increase bonding between ceramic TBC layer and metallic base materials.

1.4 Scope of the project

The work presented in this thesis is part of a joint project between Linköping University, Siemens Industrial Turbomachinery AB and Swedish Energy Agency through KME consortium - ELFORSK. The project aims at optimization of durable MCrAlX coatings for the operation conditions in land based gas turbines of medium size (10-60 MW). Such gas turbines used for both static load (long loading duration at high temperatures but few cycles) and peak load (frequent cycles) operations, require MCrAlX coatings with both long-term oxidation and thermal cycling resistance. This thesis work mainly focuses on two oxidation related issues: post-deposition surface treatments effect and coating lifetime evaluation. To gain better understandings of these two issues, oxidation tests were performed for different time period, including initial stage, inter-medium stage and long-term stage. Extensive characterization using different techniques and thermodynamic modeling were applied to investigate the coating behaviour during oxidation.

The main research objectives at current stage are given below:

1. To investigate surface treatment effects on initial oxidation stages and inter-medium stage;

2. To study the oxide scale and microstructural evolution of MCrAlX coatings at inter-medium oxidation stage;

3. To build a coating life criterion for long-term oxidation.

CHAPTER 2

MCrAlX Coatings

2.1 Coating development in historical perspective

Generally, Ni-based superalloys contained low chromium and aluminum content are less resistance to high temperature oxidation and corrosion in the service environment. Therefore, high chromium and aluminum content diffusion coatings and MCrAlX coatings are applied to improve oxidation and corrosion properties of the alloys. They can be utilized as overlay coatings and as bond coats in TBC systems. A prolonged service life of coated turbine blades can be achieved compared with the uncoated counterparts [3, 9–11]. Typical morphologies of the cross sections of coatings are shown in Fig. 2.1.

At the early stage of coating development in the late 1950s, diffusion coatings, i.e, aluminide coatings, are widely explored and still active used today [13, 14], as a result of the low cost and various well-developed processing techniques, such as slurry cementation, powder pack cementation and chemical vapor deposition (CVD). Typically, aluminide coatings contain in excess of 30 % of Al and are deposited in thickness between 30-100 μm depending on the the type of aluminide formed, as shown in Fig. 2.1a. Aluminide coatings are produced by enriching the surface with several elements at a substrate surface [15]. For instance, it can be produced by the reaction between the surface Al source and superalloy

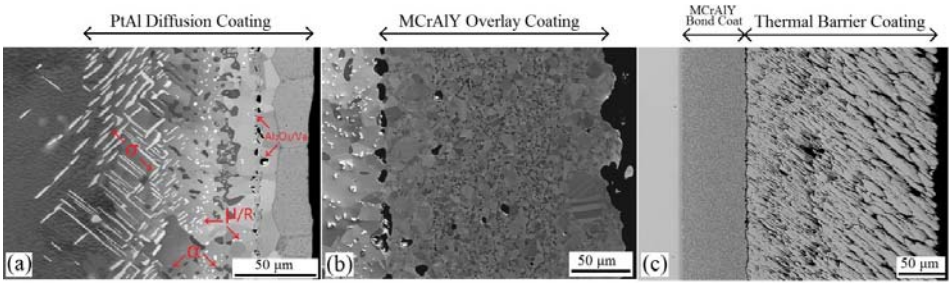

Figure 2.1. Cross sections of high-temperature coatings: (a) NiAl diffusion coating deposited by CVD, (b) MCrAlY overlay coating sprayed by HVOF, and (c) TBC deposited by EB-PVD (MCrAlY as a bond coat deposited by EB-PVD). [12]

substrates followed by inward Al diffusion and outward Ni diffusion depending on the aluminium activity during the aluminization process. When Al content at the substrate surface is low and aluminization temperature is high (>1000 ℃), the outward diffusion of Ni prevails, creating an outward diffusion coating. On the contrary, an inward diffusion coating is produced when Al content is high and temperature is low (<950 ℃) [15]. Therefore, the microstructure of aluminide coatings is highly depended on substrates by the nature of their formation. Besides, aluminide coatings offer only limited protection under hot corrosion conditions or at temperature exceeded 1050 ℃ [13]. To address these issues, MCrAlY coatings are developed to meet the demands of increasing operation temperature of modern gas-turbines.

MCrAlY coatings, with a good balance between oxidation, hot corrosion and ductility compared with aluminide coatings, draw much attentions since the early 1970s. MCrAlY coatings are alloys based on Ni and/or Co containing 15-22 wt.% Cr additions and 7.5-12 wt.% Al additions and Y levels around 0.5 wt.%, which provide good resistance against oxidation and hot corrosion. Traditionally, the term of "MCrAlY" commonly refers to the alloy or coating containing Cr, Al, Y with balancing of Ni and/or Co. Y is the most important reactive elements in MCrAlY coating, because it modifies alumina growth mechanisms and improves its adhesion against spallation [15]. Recently, the term "MCrAlX" has also been used to represent the same coating system, since other alloying elements are also added to improve coating performance. By fine modification the minor additions of oxygen-active elements like Y, Si, Hf or Ta [15–18], or a precious metal, such as Pt, Ru or Re [19–21], a good balance between oxidation, corrosion resistance

and ductility of MCrAlX coatings can be achieved. Thus, it's reasonable to name the coating system as "MCrAlX" with "X" representing all minor alloying element additions, which has been used by other researchers [22, 23]. Considering the origin and history of coating development, the use of "MCrAlY" is still adapted in the following chapters.

Thermal barrier coatings (TBCs) have been used to provide thermal insulation for the intermediate bond coat (MCrAlY) and base materials against hot gas in hot sections of gas turbine, such as combustor, turbine blades and vanes. TBCs can provide a temperature decrease in a range of 200-300 ℃ at the component surface depending on the thickness and thermal conductivity of the TBCs [15, 24]. Yttria partially stabilized zirconia is the most commonly applied TBC materials in industrial gas turbines, due to its low thermal conductivity, relative large thermal expansion, and advisable price [15, 25, 26]. The microstructure of TBC can be modified to achieve a better thermal insulation, i.e. a lower thermal conductivity, and a better strain tolerance, i.e. columnar structure as shown in Fig. 2.1c [15, 24]. A critical failure mode of TBCs is the spallation of top coat from bond coat, therefore, the surface roughness of the bond coat and quality of TGO are important [25].

2.2 Deposition Techniques

MCrAlY coatings have been deposited using a number of techniques, such as 1) plasma deposition: atmospheric plasma spraying (APS), low-pressure plasma spraying (LPPS), vacuum plasma spraying (VPS); 2) sputtering: chemical vapor deposition (CVD), electron-beam physical vapor deposition (EB-PVD); 3) flame spraying: high velocity oxy-fuel spraying (HVOF), high velocity air-fuel spraying (HVAF), 4) cold spraying and so on [27–31]. Flame spraying techniques can produce coatings comparable to other deposition techniques with a proper selection of the process parameter. Due to its low restriction of process, i.e. conduct in atmosphere instead of vacuum, production costs of thermal spraying are considerably lower [29]. In this project, the MCrAlY coatings were manufactured by HVOF and HVAF. The process of HVOF/HVAF is schematically described in Fig. 2.2. Injecting the feeding powders in carrier gas which consists of oxygen (or air) and fuel in the combustion chamber, and spraying the powders with high velocity on the target. The high speed and temperature of gas flow cause the powder particles

to be semi-melted when impacting the target surface, and the continuous spraying process leads to the formation of a typical "splat-on-splat" structure, as presented in Fig. 2.3. The moving of spraying nozzle or rotation of target eventually guarantees an even layer of compact coating with desired thickness on target materials. Post heat treatments are performed including a two-hour solution treatment at 1120 °C in vacuum and an ageing process at 845 °C for 24 h in air [32]. Such a heat treatment intends to strengthen the IN-792 substrate by refining γ' precipitates distribution and size [33], also increases the bond strength between the coating and substrate and produces dense coatings with porosity less than 1 % [34].

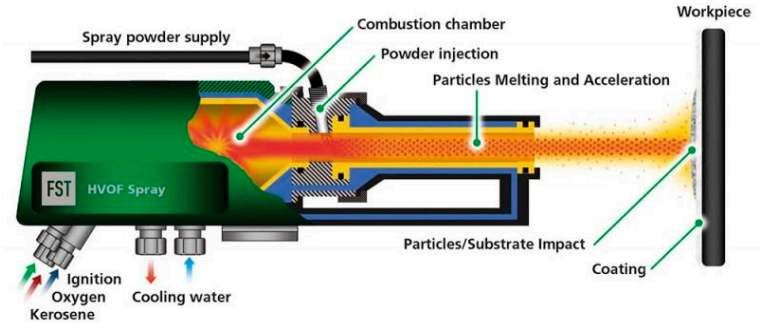

Figure 2.2. Schematic illustration of HVOF spraying process, courtesy of METHU.

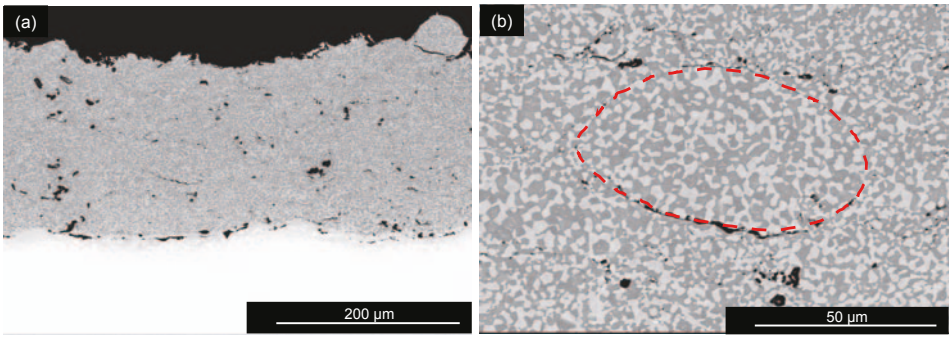

Figure 2.3. Cross sectional microstructure of an as-sprayed MCrAlY coating by HVOF spraying a) overview, b) a magnified image showing "splat-on-splat" structure (one splat marked with red circle) and cracks, voids between splats.

2.3 Oxidation

In the COMBUSTOR and TURBINE sections of gas turbines, components serve at a high temperature oxygen-containing condition and thus suffer from considerable oxidation attacks [35]. MCrAlY coatings provide resistance against oxidation for components by forming a stable, dense, continuous, slow-growing and adherent thermally grown α-Al_2O_3 layer [36–38]. The oxide scale acts as a diffusion barrier to suppress the inward diffusion of oxygen and outward diffusion of other species from coating, therefore slows down the degradation of materials. The oxidation process of coating can be divided into three stages: initial stage, steady stage and close-to-end stage, as schematically shown in Fig. 2.4a. However, the formation of other oxide species are also thermodynamically feasible as suggested by the Ellingham diagram in Fig. 2.4b. These oxides, including Cr_2O_3 and/or NiO mixed with Al_2O_3 spinel type oxides, are less-desired because they are non-protective and may promote the crack nucleation during thermal exposure of TBC [39–41]. It should be pointed out that the formation of Cr_2O_3 is protective against hot corrosion. Details of oxidation related issues will be further discussed in next chapter.

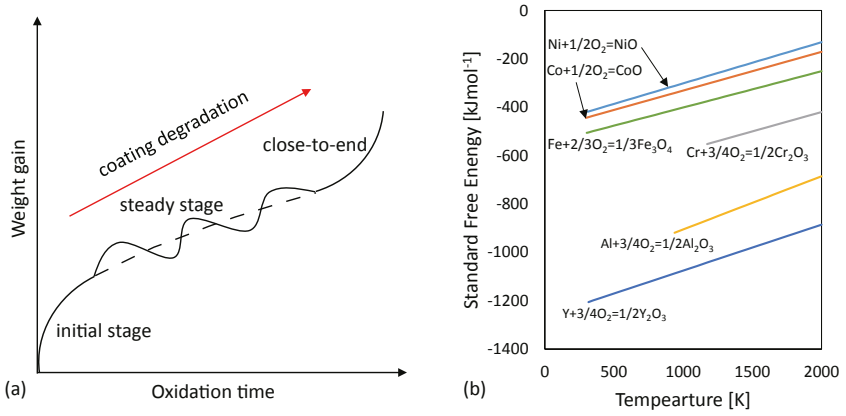

Figure 2.4. a) Schematic illustration of the three stage coating degradation due to oxidation based on [42], b) Ellingham diagram showing the Standard Free Energy of formation of oxides as a function of temperature [43].

2.4 Hot Corrosion

Hot corrosion of metals or alloys is an accelerated damage process compared with pure oxidation. It is due to the deposition of a thin film of molted salts, i.e., sulphates on the material surface at temperature between 650-1000 ℃ in gas turbines [44–46]. Two types of hot corrosion are commonly observed: Type I at 800-950 ℃ and Type II at lower temperature between 600-800 ℃, as shown in Fig. 2.5. Type I hot corrosion occurs when salts like $(Na,K)_2SO_4$ are melted to dissolve oxide scale. This process usually produces a porous oxide scale leaving the underlying alloy/coating with sulfidation penetration [47]. Type II hot corrosion occur at lower temperature, commonly presents a pitting attack with less sulfidation [15]. The damage induced by hot corrosion depends on many factors such as coating composition, thermomechanical condition, contaminant species, flux rate, temperature, salt deposition rate, gas composition, gas low rate and erosion [44]. For example, the mixture of different corrosive salts may reduce the eutectic melting point, which expands the temperature range of the hot corrosion attack. The presence of $NaCl/V_2O_5$ with sulfates further reduces the eutectic melting point of salt mixture [44, 47, 48], leading a severe attack at a lower temperature.

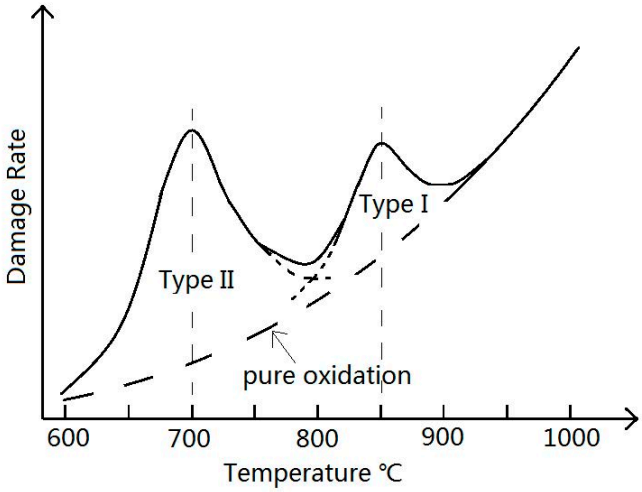

Figure 2.5. Schematic illustration of hot corrosion type I and type II superimposed on contribution of pure oxidation at different temperature regime [15, 47].

Even though the true mechanisms of hot corrosion is not well understood yet, a commonly accepted mechanism is explained by fluxing of the oxides in molten

salts due to the gradient of their solubility through the salt film thickness [15, 46, 47]. The most commonly observed corrosive salt in gas turbines is Na_2SO_4 [49–52], and the fluxing can be driven in two conditions based on the acidity or basicity of the molten salts, which can be described in Eqs. 2.1 and 2.2. The acidity or basicity of the molten salts is controlled by the temperature and gas composition (SO_3) of service condition [15, 46].

$$(Basic\ fluxing) Na_2O + Al_2O_3 = 2NaAlO_2 \tag{2.1}$$

$$(Acidic\ fluxing) Al_2O_3 + 3SO_3 = Al_2(SO_4)_3 \tag{2.2}$$

2.5 Coating-Superalloy System

2.5.1 Superalloys

Many components in gas turbine need to withstand both extreme loads and temperature during service. Ni-based superalloys show good mechanical and chemical properties at the temperatures above 0.6 times its melting point, including high strength, creep and moderate oxidation resistance at high temperature [53]. Ni is stable, since there's no phase transformation of its face centered cubic (FCC) structure from room temperature to melting point at 1455 ℃, and has a high solubility for the alloying elements. The FCC matrix of Ni-based superalloy can be strengthened by dissolution of alloying elements to form strengthening precipitates γ' phase and/or carbides or dispersive oxide-particles like Y_2O_3 [3]. Turbine disc alloys are commonly wrought in poly-crystal form, while DS (directionally solidified) or single-crystal form is often used in turbine blades. DS turbine blades have longitude grains oriented parallel to the axial direction of the blade; while single-crystal blades consist one grain.

In this project, Inconel 792, a Ni-based polycrystalline superalloy, is used as substrate. Its composition and heat treatment processes are listed in Table. 2.1. Due to the complex alloying elements, several phases can form. These phases include disordered FCC-γ phase matrix, ordered FCC-γ', carbides (MC or $M_{23}C_7$) depending on the carbon contents and TCP phases (σ, μ and etc.), which should be controlled to a limited content with the consideration of material ductility.

Table 2.1. The composition (wt.%) of Inconel 792 and heat treatment process.

Compositions	Ni	Cr	Co	W	Ta	Ti	Al	Mo	C	Zr	B
(wt.%)	Bal.	12.5	9.0	4.2	4.2	4.0	3.4	1.9	0.08	0.018	0.015
Heat treatment processes	Solution annealing (1120±10) ℃ for 2 hours in vacuum; Ageing: (845±10) ℃ for 24 hours [33].										

2.5.2 Interdiffusion between coating and superalloy

For alumina-former MCrAlY coatings, the Al content is important for an effective coating life. Aluminum in MCrAlY coatings is mainly consumed by two ways: formation of alumina scale at coating/gas interface and inward diffusion of Al from coating to substrate. Interdiffusion inevitably occurs through coating/substrate interface during service at high temperature inducing microstructure evolution, due to the alloying element gradient between MCrAlY coatings and superalloy substrates. It leads to microstructure changes near the interface depending on the temperature, and composition of both coating and substrate. Such microstructural changes at coating/substrate interface may affect the mechanical behavior of the coating-substrate system. Besides, interdiffusion consumes Al content of coating, reducing coating life. As shown in Fig. 2.6, interdiffusion induced microstructural evolution can be readily observed after 10,000 h oxidation compared with that of 2000 h.

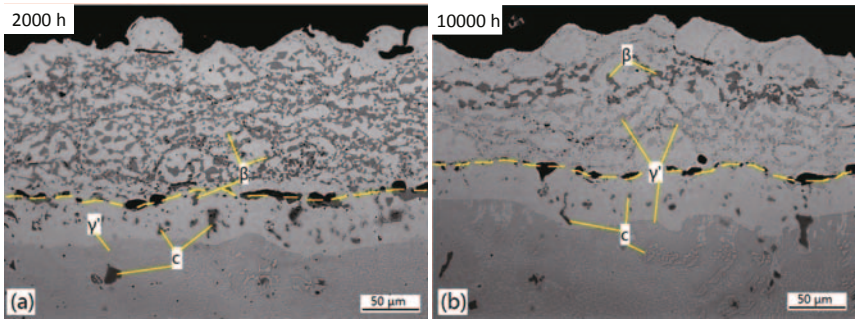

Figure 2.6. The cross sections of MCrAlY coating after the oxidation for (a) 2000 h and (b) 10,000 h. Coating/substrate marked by dash line [32].

CHAPTER 3

High Temperature Oxidation

3.1 Oxidation theory

When a clean metal M is exposed to an oxidizing environment, it reacts with oxygen gas, forming an oxide scale, which can be expressed as:

$$xM(s) + (y/2)O_2 = M_xO_y \tag{3.1}$$

The formation rate and properties determine its protectiveness. In general, a protective oxide should be thin, dense, slow-grown, adhesive to the metal, and thermodynamically stable within the working temperature range. Not all oxidation reactions occur spontaneously, which is decided by the free energy of formation of oxides, ΔG. Only the reaction with negative ΔG can occur spontaneously [11], as presented in Fig. 2.4b.

As illustrated in Fig. 3.1, the initial stage of oxidation reaction between metal and oxygen basically can be described in the following steps: 1) absorption of oxygen at the metal surface, 2) dissolution of oxygen in metal and separated oxide islands nucleation on the surface, 3) lateral growth of oxide islands to form a continuous oxide film of M_xO_y form. The oxide film formed can be dense and defect-free which serves as diffusion barrier between metal and reactants, i.e. the oxidation can only proceed with solid-state diffusion through oxide film. However,

porous oxides can be formed, in which pores provide fast diffusion paths for the transportation of metal and oxygen ions. Due to the high mobility of oxygen ions, the oxidation is much faster; it cannot be slowed down unless a new barrier is built-up forming a dense and stable oxide layer.

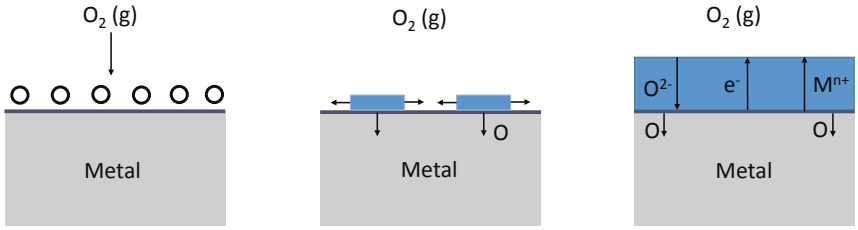

Figure 3.1. Schematic representation of oxide scale formation at initial stage. Adapted from [54].

3.2 Solid-state diffusion mechanism

The growth of thick oxide scales at elevated temperatures is in principle governed by diffusion of ions and electrons through the scale, which depends on the defects in the oxides. Based on the defect types, the diffusion mechanisms can be sorted into bulk diffusion (lattice diffusion) and short-circuit diffusion. Among three groups of defects, including point defects, line defects and plane defects, point defects are responsible for lattice diffusion and the rest for short-circuit diffusion. However, the relative contributions to the scale growth by bulk or grain-boundary diffusion depend on the oxidation temperature and scale thickness [55]. Wagner refined Tammann's mechanisms on the oxidation of metals and proposed famous Wagner's model, as shown in Fig. 3.2. The charged species can either diffuse through the lattice of oxides, or along 'short-circuit' paths.

Aluminium is one of the two common metals that form nearly stoichiometric oxides. Schottky and Frenkel defects are two common existed defects in stoichiometric crystals, as illustrated in Fig. 3.3. A Schottky defect is formed by equivalent concentrations of anion and cation vacancies in the structure. On the other hand, Frenkel defect forms when a metal ions moves from the cation lattice to an interstitial site, leaving a metal vacancy on the regular site.

The non-stoichiometric oxides are more common in metal oxides. which are classified as oxygen or cation defects (deficit or excess). More specifically, metal

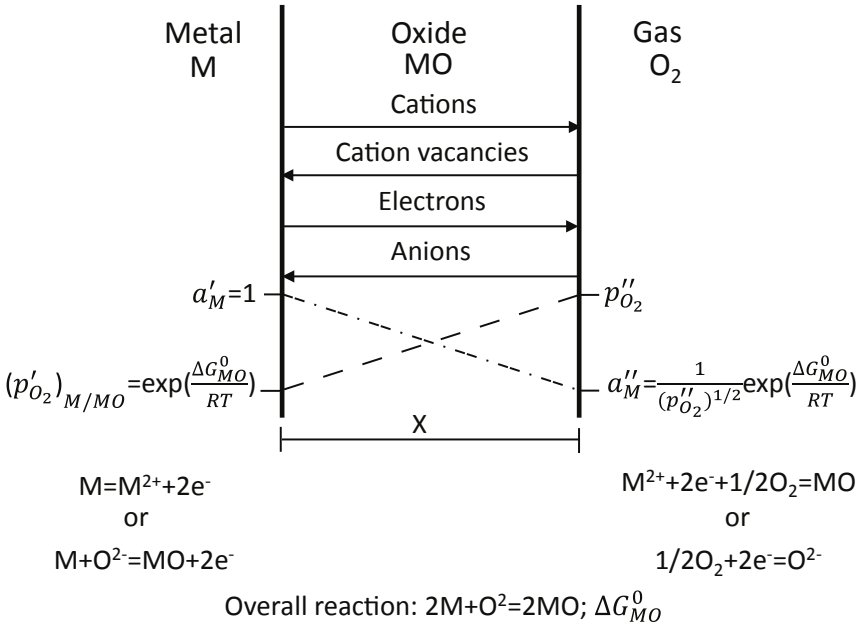

Figure 3.2. Diagram of scale formation according to Wagner's model [55].

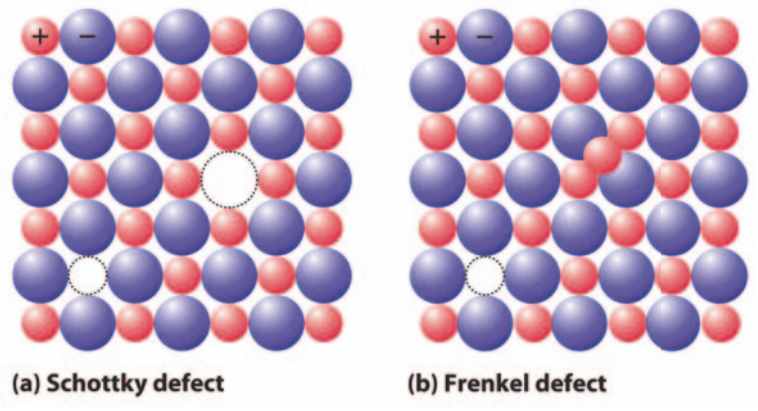

Figure 3.3. Defects in ionic crystals. [4]

excess compensated by metal interstitial or oxygen deficit compensated by oxygen vacancies are n-type, metal deficit compensated by metal vacancies or oxygen excess compensated by oxygen interstitial are p-type.

Other than point defects, reaction species also diffuse through grain boundaries, dislocation clusters and continuous pores or cracks, which requires only 50-70 % of the activation energy of the lattice diffusion. In addition, the diffusion coefficients are 10^4-10^6 times larger than lattice diffusion coefficients [54]. This type of diffusion contains high diffusivity paths often referred as short-circuit diffusion. In general, the short-circuit diffusion is more dominant at relative lower temperature, while less effective at higher temperature. Short-circuit diffusion is the main diffusion mechanism for Al_2O_3 also in the high temperature range for the rather low point defect concentrations [56]. For instance, the oxide grain boundaries lead to a thickening of the oxide above and below the oxide on either side of the boundary, as shown in Fig. 3.4.

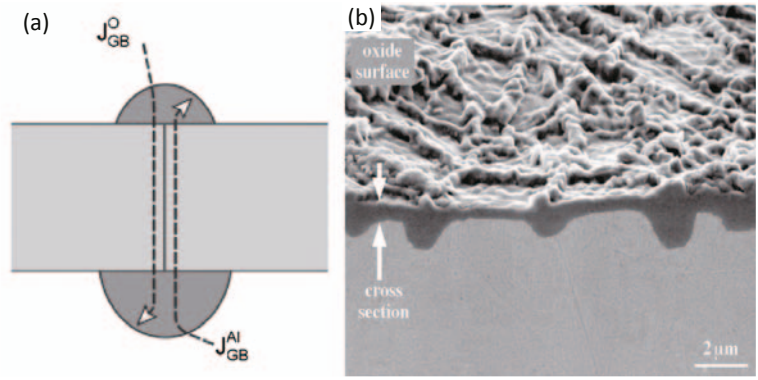

Figure 3.4. Illustration of alumina formed on polished surface. Schematic of the counter-diffusion of O and Al along the oxide grain boundaries leading to a thickening of the oxide above and below the oxide on either side of the boundary. In between grain boundaries, the oxide is significantly thinner as indicated by the arrows. [57]

3.3 Basic oxidation kinetics

The oxidation kinetics can be determined by measuring the weight gain or oxide thickness. Generally, three oxidation behaviors are observed: parabolic, logarithmic and linear, see Fig. 3.5.

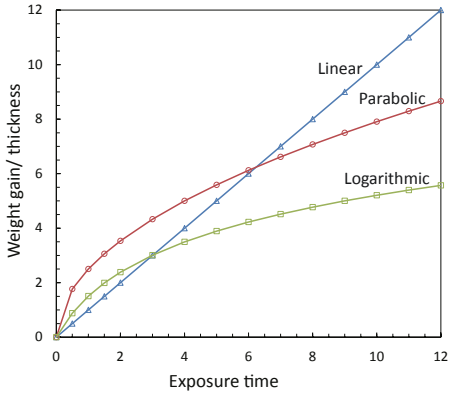

Figure 3.5. Weight gain or oxide thickness for the kinetic rate of oxidation [58].

3.3.1 Parabolic oxidation

At high oxidation temperature, the growth rate of most metal oxides follows the parabolic kinetic law, see Fig. 3.5. Such an oxidation behavior indicates that the growth of oxide is proportional to the time t:

$$x^2 = k_p t, \tag{3.2}$$

where x can be mass gain or oxide thickness, k_p is the parabolic rate constant, and t is the oxidation time [58]. Some assumptions have been made to fulfill the condition of parabolic law: the oxide scale is compact and good adherent; transportation of ions through oxide scale is rate controlled; thermodynamic equilibrium is established at each interface, i.e. gas/oxide and oxide/metal. In general, the parabolic law applies to high temperature oxidation, where the oxide growth is controlled by the diffusion of reaction species through relatively thick oxide scale.

3.3.2 Logarithmic oxidation

When metals are oxidized under certain conditions, typically at low temperatures up to about 400 ℃, the initial oxide formation, up to the 1000 Å range, is characterized by an initial rapid reaction that quickly reduces to a very low rate of reaction [55]. Such behavior follows the logarithmic kinetic law:

$$x = k_{log} log(t + t_0), \tag{3.3}$$

where x is the oxide thickness, k_{log} is the logarithmic rate constant, t is the oxidation time, and t_0 is a constant. When the oxide scale grows thicker, the parabolic kinetics usually takes over.

Besides, it was reported by Lipkin et al [59] that the lateral growth of α-Al_2O_3 on NiAl at 1100 ℃ also obeyed the logarithmic law, as presented in Fig 3.6. It indicates that the α-Al_2O_3 nucleates within the θ-Al_2O_3 and grows laterally by the radial migration of the transformation front until impingement.

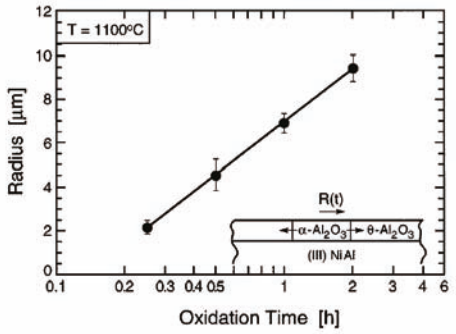

Figure 3.6. The measured mean radius of α-Al_2O_3 islands plotted as a function of oxidation time. As the least squares fit demonstrates, the θ–to–α transformation follows logarithmic kinetics. [59]

3.3.3 Linear oxidation

Under certain conditions the oxidation rate of a metal proceeds at a constant rate and is proportional to the oxidation time following a linear rate law:

$$x = k_l t, \tag{3.4}$$

where x is the oxide thickness or mass grain, k_l is linear rate constant, and t is the oxidation time. It could happen at early stage of oxidation when the scale is thin and a phase-boundary process is the rate determining step for the reaction [55]. In addition, the existence of micro crack or porosity in oxide scale could transform the oxide growth from parabolic to linear. Such behavior are commonly observed when a protective scale breaks down at a continuously increasing number of sites, resulting in an increased oxidation rate, which is called “breakaway” [58].

CHAPTER 4

Oxidation of MCrAlX coating

Al_2O_3-forming MCrAlY coatings can exhibit good resistance against high temperature oxidation by forming a continuous α-Al_2O_3 layer. The oxidation of MCrAlY coatings can be divided in three stages, as introduced in Fig. 2.4a. This chapter addresses the oxidation related issues regarding MCrAlY coatings which are the main focuses of this thesis. Surface treatment effects on coating oxidation are described followed by an Al-activity based coating life criterion.

4.1 Various oxides

In the case of oxidation of MCrAlY, alloying elements can be oxidized, forming various oxide species at initial oxidation stage. These oxides include transient and stable Al_2O_3, Y-oxides, Cr_2O_3 and/or NiO mixed with Al_2O_3 spinel type oxides, and their formation depends on many factors, including the oxidation temperature, alloying composition, coating microstructure, and surface condition.

4.1.1 Alumina phases

During oxidation of MCrAlY coatings, Al_2O_3 can be formed in different crystallographic phases. At lower temperatures or in the early stage of oxidation, the

formation of metastable γ-Al_2O_3, δ-Al_2O_3 and θ-Al_2O_3 are often observed, which contain high concentrations of cation vacancies. These metastable oxides show distinctive morphological features and have a higher growth rate compared with α-Al_2O_3, and their transformation to α-Al_2O_3 may take a long time, allowing the preservation of their features [60]. Unlike metastable alumina, due to the large band gap and high lattice energy, the concentrations of ionic and electronic defects in α-Al_2O_3 are extremely small [54]. α-Al_2O_3 exhibits low diffusivity for cations and anions as well as low oxide growth rate as a result of nearly perfect stoichiometry. Hence, the formation of stable α-Al_2O_3 scale is desired for its low oxide growth rate and the defect-free stoichiometric structure enable α-Al_2O_3 to serve as protective oxide scales for high temperature application.

The metastable transient alumina is not widely reported since these phases appear only after short exposure times at relatively low temperatures. They eventually transfer to stable α-Al_2O_3 with prolonged oxidation time. Table 4.1 shows the details of the crystal structures of alumina phases. Transient alumina contains high concentrations of vacancies and lattice defects, resulting in a fast outward growth behaviour by outward diffusion of aluminum cations. For instance, the growth rate of θ-Al_2O_3 is about an order of magnitude higher than α-Al_2O_3 [61]. α-Al_2O_3, has a corundum structure, is the most stable alumina phase. It transformed from the metastable phases, and the transformation rate depends on various factors, such as temperature, surface condition, alloying elements and so on. The transformation sequence of alumina phases, depending on temperature, can be expressed as [62–64]:

$$\gamma \xrightarrow{750^\circ C} \delta \xrightarrow{900^\circ C} \theta \xrightarrow{1000^\circ C} \alpha\text{-}Al_2O_3 \tag{4.1}$$

4.1.2 Other oxides

Y-oxide

Yttrium is added to MCrAlY coating in only small amounts (0.3-0.5 wt.%), in order to improve the adhesion of the oxide scales to the coating [66]. Due to its high affinity to oxygen, Y-oxide pegs are commonly observed in oxide scale formed on MCrAlY coatings, where oxide/coating interface and oxide grain boundaries are preferential segregation sites [67]. In HVOF/HVAF coatings, which are deposited at atmospheric pressure, all Y is bonded to oxygen [68]. On the contrary,

Table 4.1. Crystal structure of the main alumina phases [65].

Al_2O_3 phase	Crystal system	Lattice parameters (Å)	Oxygen sub-lattice
γ-Al_2O_3	Cubic	a=7.991	fcc
δ-Al_2O_3	Tetragonal	a=7.96, c=11.7	fcc
θ-Al_2O_3	Monoclinic	a=5.64, b=2.92, c=11.83, β=104 °	fcc
α-Al_2O_3	Rhombohedral Hexagonal	a=4.7589, c=12.991	hcp

in the case of EB-PVD deposition under high vacuum, the Y in MCrAlY coatings usually presented as metallic M_5Y precipitates along grain boundaries after coating deposition [69]. The positive effect of Y addition can be explained by reactive element theory, i.e., Y scavenges impurities like sulfur for its segregation to the coating/oxide interface causes a significant decrease in scale adhesion [70–72]. Besides, the presence of Y-oxide can also significantly promote the formation of α-Al_2O_3, suppress formation of voids at the oxide/coating interface, modify the growth rate of the alumina scale, and increase oxide/coating adhesion due to the formation of inward-grown oxide protrusions (also called pegs) [66]. Fig. 4.1 shows Y-oxide segregates at gain boundaries of alumina oxide formed on a HVOF sprayed MCrAlY coating.

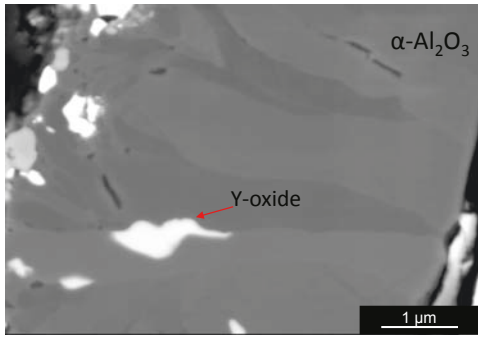

Figure 4.1. Y-oxide segregation at alumina oxide grain boundaries.

Spinel

The formation of spinel type, $(Ni,Co)(Al,Cr)_2O_4$, above the alumina scale is commonly observed during oxidation of MCrAlY coatings, as shown in Fig. 4.2. The structure of spinel depends on oxidation temperature, i.e., spinel tends to have a Cr-dominate $(Ni,Co)Cr_2O_4$ structure at lower oxidation temperature, but a Al-dominate $(Ni,Co)Al_2O_4$ structure at higher oxidation temperature [73]. The transition from $(Ni,Co)Cr_2O_4$ to $(Ni,Co)Al_2O_4$ when increasing temperature can be due to an evaporation of Cr at the higher temperatures [74].

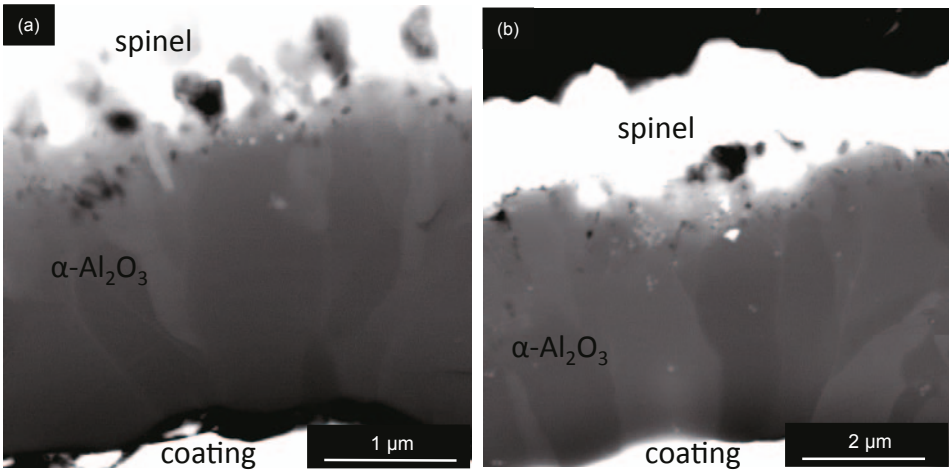

Figure 4.2. Cross section of TGO formed on MCrAlY coating at 1000 ℃ oxidation for 500 h (a) and 5000 h (b). (Note that the images are in different magnifications.)

4.2 Three stage oxidation

4.2.1 Initial Stage

Prior to the formation of stable α-Al_2O_3, metastable alumina oxides, such as γ and θ-Al_2O_3, develop rapidly showing distinctive morphological features. Considering their higher growth rate compared with α-Al_2O_3, the rate of transient-to-α-Al_2O_3 phase transformation has a significant impact on oxide scale microstructure, which controls the overall growth rate of alumina scale at the initial oxidation stage. Therefore, a fast transformation from transient oxides to the protective α-Al_2O_3 reduces the overall oxide growth rate, hence the better long-term coating perfor-

mance of the coating. By the nucleation of α-Al_2O_3 at oxide/coating interface, α-Al_2O_3 grows outward by consuming transient oxides, in this way completing the transient-to-α-Al_2O_3 transformation [60]. In the meantime, the lateral growth of α-Al_2O_3 nucleate islands also occurs till the impingement, forming a compact α-Al_2O_3 scale. A two-layer alumina scale consisting of an inward-grown inner α-Al_2O_3 layer and an outer layer transformed from outward-grown transient alumina can be observed, as shown in Fig. 4.3.

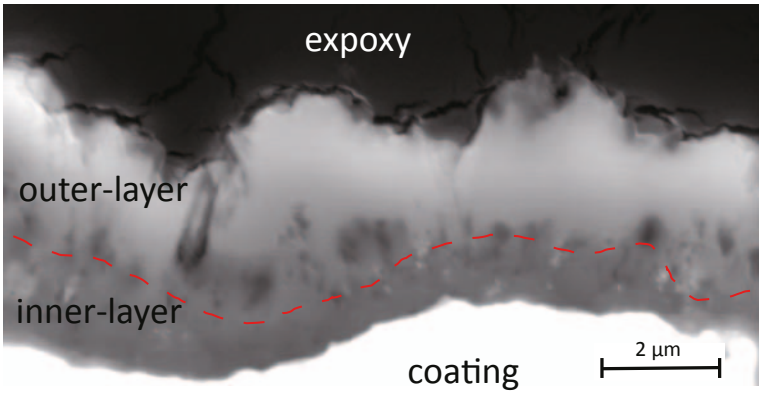

Figure 4.3. Cross section of TGO showing a two-layer structure, interface of two layers marked in dash line [60].

4.2.2 Steady Stage

Growth of Oxide Scale

After initial oxidation stage, α-Al_2O_3 develops into an elongated compact fine columnar structure, as shown in Fig. 4.2. According to Brady et al. [75], doping with REs such as Y, Hf , La and Zr in MCrAlY coating had some significant effects on improving thick oxide scale to develop a columnar morphology. The presence of REs oxide segregation at grain boundaries of α-Al_2O_3 converts the oxide growth mechanism from outward growth to inward growth by suppressing Al outward diffusion through oxide scale [37]. With further oxidation at steady stage, alumina scale continues to grow inward with well-preserved columnar structure. Once the TGO thickness reaches a critical level, the “breakaway” oxidation initiates due to the mismatch stress build-up. After each breakaway, parabolic growth continues, eventually leads to complete spall or a linear growth profile [15], as illustrated in

Fig. 2.4a.

Microstructure Degradation of Coating

As shown in Fig. 2.6, due to the consumption of Al in coating during oxidation, the β phase (high Al content) transforms into γ' (medium Al content) or γ (low Al content) following:

$$\beta + \gamma \rightarrow \beta + (\gamma') + \gamma \rightarrow (\gamma') + \gamma, \tag{4.2}$$

while the stability of γ' phase in coating depends on coating composition and temperature. If γ' phase is not stable in the coating, β phase would transform into γ phase directly. The depletion of β phase leads to the formation of an outer beta phase depletion zone (OBDZ) in the coating below the coating/oxide interface due to oxidation at coating surface, and an inner beta phase depletion zone (IBDZ) near the coating/substrate interface due to substrate interdiffusion, as shown in Fig. 4.4a. The oxidation resistance of MCrAlY coatings can be compared referring to the OBDZ thickness, for instance, coating C1 in Fig. 4.4b with low OBDZ thickness indicates a better oxidation resistance than C2.

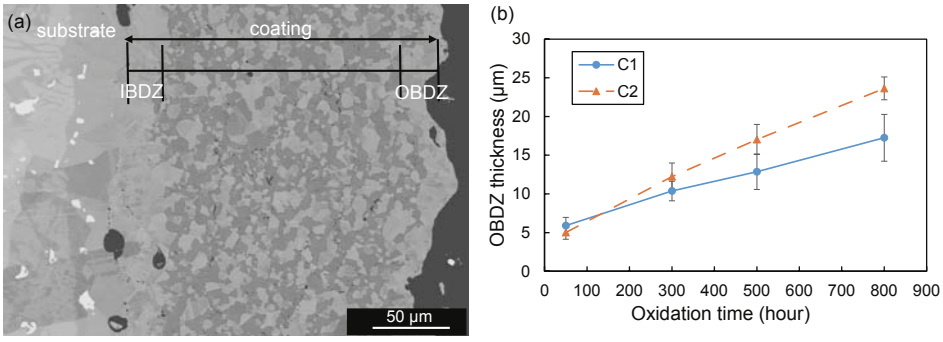

Figure 4.4. (a) Microstructure of MCrAlY coating after oxidation, (b) OBDZ thickness evolution of two MCrAlY coatings at different oxidation time.

4.2.3 Close-to-end Stage

Internal Oxidation

After long-term oxidation, Al content in MCrAlY coatings continues to decrease due to its depletion by oxidation and substrate interdiffusion. After complete

depletion of β phase, as described in Eq. 4.2, only γ phase exists in coating. When Al content reaches a critically low level, internal oxidation occurs, as shown in Fig. 4.5, indicating the end of coating life.

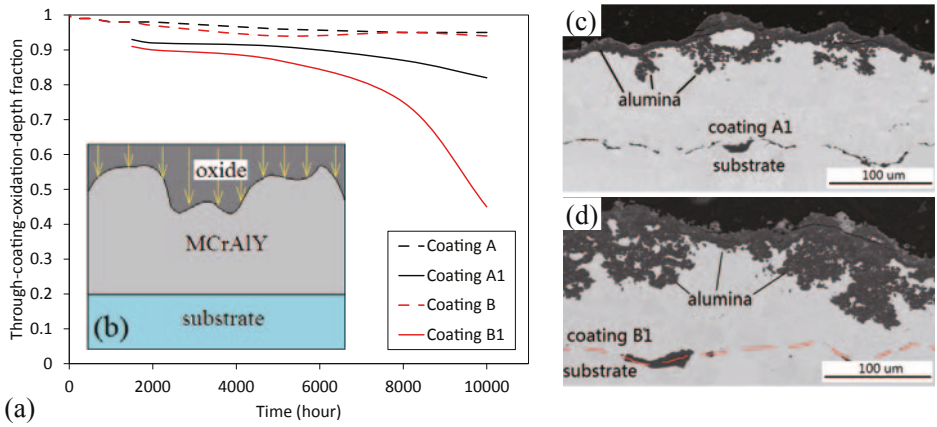

Figure 4.5. (a) The through-coating oxidation-depth fraction (a ratio between the oxidation depth and coating thickness) in coatings, (b) schematic illustration of how the oxidation depth is measured, (c) and (d) cross sections of A1 and B1 coatings after long-term oxidation, respectively.

4.3 Improving coating oxidation resistance

The drive to improve engine combustion efficiency while reducing emissions by increasing the operation temperature brings a big challenge for coating design. As a result, the need for improvement of MCrAlY coatings for better oxidation resistance is essential. Formation of a stable, dense, continuous, and slow-growing α-Al_2O_3 layer, at MCrAlY coating surface, is the key to oxidation protection, since the protective α-Al_2O_3 scale offers superior oxidation resistance due to its lower oxygen diffusion rate as compared to other oxides. The ability of a MCrAlY coating to form and maintain such a protective scale depends on the coating composition and microstructure, and can be improved through optimization of deposition parameters, modification of coating surface conditions and so on.

4.3.1 Role of alloying elements

Alloying element additions in MCrAlY coatings modify coating oxidation resistance. Extensive work [76–80] has been conducted to explore the mechanisms of REE (reactive element effect), however, many hypotheses have been proposed up to now, the mechanisms explanation is still in debate. The studies on REE continue nowadays to fulfill the increasing demand of coating design.

Large ions such as REs (reactive elements) in open cubic lattice would inhibit the martensitic transformation from cubic θ-Al_2O_3 to hexagonal α-Al_2O_3 [81]. The presence of Y in MCrAlY could suppress transient-to-α-Al_2O_3 phase transformation, leading to a fast growth of transient oxides before its transformation to α-Al_2O_3. Hence, a thick outer-layer is expected reducing the long-term coating life [60]. The addition of RE, such as Y, Hf in MCrAlY, also alters growth mechanisms of alumina scale, as mentioned in 4.1.2.

As a major elements in MCrAlY coatings, the addition of Cr is essential since it increases both coating oxidation performance and hot corrosion resistance. It reduces the Al requirement from 17 % to as low as 5 % in the Ni-Al system to form a continuous Al_2O_3 scale through gettering effect [15] or third element effect [82] described below. Due to a low solubility of Cr in β phase, most Cr in MCrAlY coatings partitions in γ matrix. The presence of Cr leads to the formation of α-Al_2O_3 at early oxidation stages and reduces the low temperature limit for forming the oxide. The formation of Cr_2O_3 islands which shares the same epitaxial template as α-Al_2O_3, thereby facilitates fast α-Al_2O_3 formation during early stage oxidation [83]. Therefore, thermally-grown Cr_2O_3 islands form readily because of sufficient Cr supply from the γ-phase and catalyze the nucleation of α-Al_2O_3. On the contrary, transient oxides formation on the β phase is less profound, as a result of the low Cr content of β phase.

Recent research trend shows some promising results of alloying element effect. It was reported by He et al. [84] that the addition of Dy brings a lower oxide scale growth rate and better bonding of scales. The addition of Re [85] or Ta [86] also enhances coating oxidation performance by lowering the oxidation rate and Al diffusivity. Ru addition in MCrAlY coating improves long-term oxidation performance by reducing substrate interdiffusion [87]. Pt addition reduces voids formation near oxide/coating interface, improving cyclic oxidation resistance [88].

4.3.2 Role of coating microstructure

By modification of coating microstructure, oxidation resistance of MCrAlY coating can be improved. For instance, by increasing the β phase fraction in MCrAlY coatings for a better long-term oxidation resistance, a gradient coating with increasing Al content from coating/substrate to surface promotes oxidation resistance of coating [89]. To decrease the Al consumption by substrate interdiffusion, deposition of a Ni-Re diffusion barrier at the coating/substrate interface can effectively reduces the Al diffusivity and the oxidation rate [90]. Besides, the nano-oxide (Al_2O_3) dispersion in coatings reduces elements diffusion from substrate to coating surface which increases coating oxidation resistance [91].

4.3.3 Role of surface treatments

A promising route to decrease the oxidation rate of MCrAlY coatings is post-deposition surface modification which can facilitate formation of a uniform alumina scale with a considerably low growth rate compared with the as-sprayed coatings. Surface treatments modify coating surface condition, which improves coating oxidation performance. Commonly used surface treatment methods include mechanical polishing [92], shot-peening [93, 94], electron beam treatment [95–98], laser-surface treatment [99, 100] and so on. The positive effects can be summarized as follows:

- decrease coating surface roughness, reduce surface/bulk ratio giving a lower oxide growth rate of overall coating;
- suppress fast growth of transient oxides, aid the transient-to-α-Al_2O_3 phase transformation;
- provide more nucleation sites of α-Al_2O_3, enable the fast development of compact α-Al_2O_3;
- suppress the formation of spinels, good for TBC application;
- reduce the overall oxide growth rate, less spallation of TGO.

It's worthy to mention the positive effect of vacuum treatment. For instance, it promotes the formation of a dense and uniform oxide layer on a HVOF sprayed coatings compared with as-sprayed [97]. Unlike the conventional surface treatment introducing cold work on coating surface, novel surface treatment methods can also

improve the oxidation resistance. For instance, by sputtering a layer of α-Al_2O_3 on MCrAlY coating surface using PVD, it reduces oxidation rate and also promotes the adhesion between MCrAlY bond coat and top coat [101].

4.3.4 Role of deposition techniques

As aforementioned, MCrAlY coatings can be produced by a number of deposition techniques. Due to the work principle of deposition techniques, different as-deposited coating microstructures are expected. The difference of microstructure can be grain size, grain orientation, phase, porosity, element distribution, coating surface roughness, oxidation rate of powder during spraying and so on. One or several reasons mentioned above can contribute to such differences. For instance, cold sprayed MCrAlY coatings show a lower β phase depletion rate during oxidation compared with that of LPPS sprayed coatings due to different element distribution and surface roughness [102].

Besides, spraying parameters of coating deposition can be tuned to achieve a better coating performance. For instance, spraying distance, powder flow, gas flow, and powder size of HVOF process have a significant influence on microstructure of coating, giving different coating oxidation performance [103]. Moreover, the impact of surface treatment on coatings oxidation resistance differs in coatings produced by different deposition techniques.

4.4 A coating life criterion

The depletion rate of β phase in MCrAlY has been used as a criterion by many investigators to evaluate the end of coating lifetime. However, the complete depletion of β phase doesn't necessarily mean the end of coating life. It was indeed observed that some Ni-Al and Ni-Cr-Al alloy systems with no beta phase presence maintain the ability to provide protection. Some researchers found from empirical studies that the concentration of Al in a range of 4–6 wt.% is often sufficient to maintain α-Al_2O_3 scales and thus to provide certain oxidation resistance. In such cases, the complete depletion of β phase is obviously not an adequate coating life criterion. The empirical Al concentration criterion also has its limitation: the minimal Al concentration required by a continuous α-Al_2O_3 scale varies with coating composition [32].

To address the issue, an Al-activity based coating life criterion is therefore

proposed by the author [32] to predict coating life. In thermodynamic theory, activity is a measure of the "effective" concentration of a species in the system which can be used to define equilibrium constant [104]. Based on Eq. 3.1, the oxidation of Al can be represented by

$$4/3Al + O_2 \rightarrow 2/3Al_2O_3, \tag{4.3}$$

and the Gibbs free energy of formation of alumina can be expanded consistent with the Van't Hoff isotherm [55] according to

$$\Delta G = \Delta G_0 - RT * ln\left(\frac{a_{Al_2O_3}^{2/3}}{a_{Al}^{4/3} * \frac{p_{O_2}}{p_{O_2}^0}}\right) = \Delta G_0 + RT * ln\Big(a_{Al}^{4/3} * \frac{p_{O_2}}{p_{O_2}^0}\Big), \tag{4.4}$$

where ΔG is Gibbs energy change of the reaction in kJ/mol, ΔG_0 is standard Gibbs energy of formation of alumina in equilibrium reaction, R is gas constant, T is temperature in Kelvin, a_{Al} is Al activity, $a_{Al_2O_3}$ is Al_2O_3 activity (commonly taken to be unity), p_{O_2} is oxygen partial pressure of oxidizing atmosphere, and $p_{O_2}^0$ is the standard pressure, equals to 1 bar. Eq. 4.4 can be transformed into a simplified Arrhenius type equation to calculate the critical Al activity of alumina formation

$$a_{Al} = A * exp\Big(-\frac{\Delta G}{RT}\Big), \tag{4.5}$$

where A is a mathematic constant. Based on the experiment results of Ni-Cr-Al, Ni-Al-Si and Ni-Al alloy systems from literature, the critical Al activity of continuous alumina formation for MCrAlY coating in Eq. 4.5 can be expressed as a function of oxidation temperature:

$$a_{Al,cri} = exp(-10,235/T - 11.1). \tag{4.6}$$

CHAPTER 5

Experimental methods

5.1 Surface treatment

Surface treatment effect on coating oxidation resistance is one of the subjects in this thesis. Three different post-deposition treatments were performed on coating surface, including mechanical polishing, shot-peening, and laser surface melting (LSM). For the polishing treatment, the as-sprayed MCrAlY samples were first ground and then polished in the following sequence: 1200 and 4000 grit silicon carbides paper, diamond suspension with particle size of 1 μm, and diamond suspension with particle size of 0.05 μm. A mirror-like surface finish was achieved after the polishing. For shot-peening treatment, samples were shot-peened using spherical glass shots (300 μm in diameter) with 150-200 % surface coverage and a shot peening intensity of 0.2 to 0.3 mmA (Almen intensity). The working pressure was 0.3 MPa and the working distance was 150 mm. For LSM treatment, sample surfaces were scanned using a 6 kW YAG fiber laser which reproduced a laser spot of 0.8 mm in diameter. Processing parameters were 400 W laser power and 25 mm/s scanning speed. Argon was used as shielding gas with a flow rate of 11.5 L/min.

5.2 Oxidation testing

In this project, oxidation tests were performed in lab air at isothermal condition (900, 1000 and 1100 ℃) or at thermal cycling condition with 1 h heating at 1100 ℃ and 10 min compressive-air cooling to 100 ℃. The testing furnaces are shown in Fig. 5.1. Most oxidation tests in this thesis were done in Siemens Industrial Turbomachinery AB (Fingspång), except that the short-term oxidation was performed in a tube furnace in Linköping University, as shown in Fig. 5.2, in oder to gain a better control of temperature and reduce the heating time.

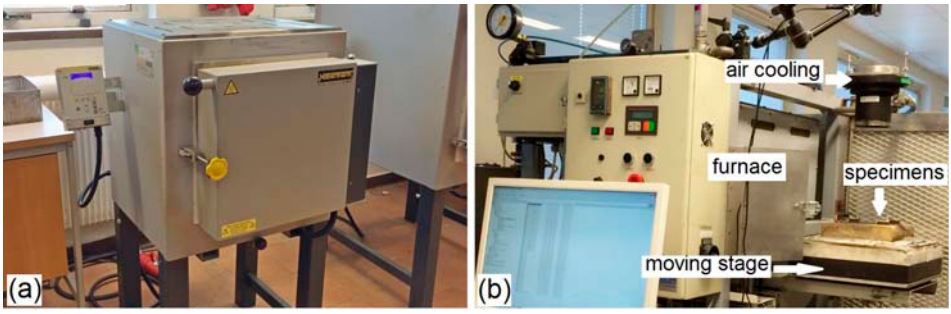

Figure 5.1. The oxidation testing furnaces for: a) isothermal oxidation, b) cyclic oxidation. Both tests were performed at Siemens Industrial Turbomachinery AB (Fingspång).

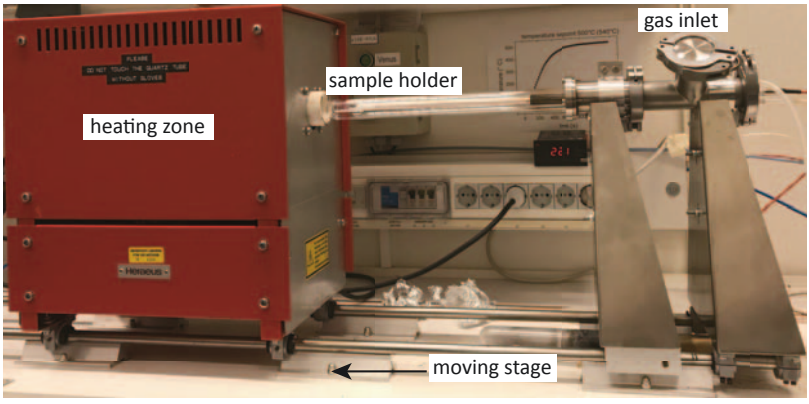

Figure 5.2. Tube furnace for short-term exposure.

5.3 PSLS

Photo-stimulated luminescence spectroscopy (PSLS) is used in materials science for the detection of "photo-emitted" light from the materials, because of the high sensitivity and non-destructive character of this technique. In a photoluminescence process, an incoming high energy light at a constant wavelength is used to illuminate the specimen to be analyzed. The incoming photos are focused on samples, and the incident energy can be absorbed when photo energy is greater than the band gap of the materials ($E>E_g$), leading to a photo-excited process. The electrons within the samples are excited to higher states, and return to a lower energy state accompanied by the emission of a photo [105].

The experiments were carried out using a Horiba Jobin Yvon integrated micro-Raman setup, as shown in Fig. 5.3a and schematic illustration of photoluminescence experiments in Fig. 5.3b. The photo-stimulated luminescence was excited by a diode laser at wavelength (λ) of 532 nm, the laser was focused using a 50x objective lens with NA=0.5 on the sample. The signal was collected using the same lens, and dispersed on a 300 mm^{-1} grating and collected with a Horiba Synapse Peltier-cooled charge-coupled device (CCD). The recorded spectra were analyzed and fitted using commercial Origin software. The fitting of spectral peaks with a combination of peaks are based on Levenberg-Marquardt non-linear peak method [106].

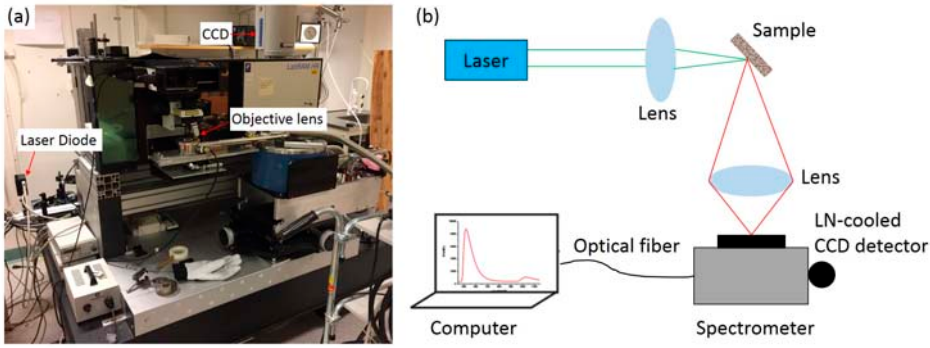

Figure 5.3. (a) Overview of PSLS setup used in this thesis, (b) diagram of the photoluminescence experiment.

Table 5.1. Characteristic luminescence peak positions of Cr-doped α-Al_2O_3 and θ-Al_2O_3 in stress-free state.

Cr-doped doublet	Peak position (cm^{-1})
R1	14,402
R2	14,432
Q1	14,564
Q2	14,626

5.3.1 Identification of Alumina phases by PSLS

Due to the dopping of Cr^{3+} in α-Al_2O_3, Cr^{3+} ions substitute Al^{3+} site in the octahedral coordination giving a strong luminescence [107], which can be identified by PSLS. The origin of the luminescence is the photo-stimulation and subsequent radiative decay of excited d^3 electrons in substitutinal Cr^{3+} ions located on octahedral sites [108, 109]. And Cr^{3+} ions substitution of Al^{3+} site in octahedral (θ-Al_2O_3) and tetrahedral sites (γ-Al_2O_3) can also generate characteristic luminescence [110]. Characteristic lines of Cr-doped α-Al_2O_3 (R1-R2 doublet) and θ-Al_2O_3 (Q1-Q2 doublet) can be observed, and their peak positions are listed in Table 5.1.

5.3.2 Piezospectroscopic Effect

Compressive residual stresses in alumina scale mainly originate from the relatively low thermal expansion coefficient of the scale compared with metallic coating substrate during cooling [111]. The characteristic lines result from the electronic transitions of the dopant ions are extremely sensitive to the local ionic environment in the host crystal as described by Ligand field theory. As a result, deformation which alters the interionic distances can cause shifts in the characteristic luminescence lines. Also, deformation which reduces the symmetry of the crystal will remove the existing degeneracy of the energy states and thereby lead to splitting as well as shifting of lines in the spectra [112]. The relation between strain (equivalently stress) and the change in energy of the electronic states is the piezospectroscopic effect. This relationship between an observed line shift in a fluorescence or absorption spectrum and the state of stress was first described phenomenologically

by Grabner [113].

The relationship between the fluorescence frequency shift, $\Delta\nu$, and the local stress can be expressed to a first-order approximation, as

$$\Delta\nu_{stress} = \prod_{ij} \sigma_{ij}^{c} = \prod_{ij} a_{ki} a_{lj} \sigma_{kl}, \tag{5.1}$$

where $\prod_{ij}$ is the ijth component of the piezospectroscopic tensor and σ_{ij}^{c} is the stress state in the crystallographic basis of the host crystal. In a general coordinate system, the stress state, σ_{ij}, is related to σ_{ij}^{c} by the transformation matrix, a_{ij}. The piezospectroscopic tensor is a material-specific parameter that reflects the point symmetry of the fluorescing ion in the host lattice. The coefficients of the piezospectroscopic tensor were redetermined with greater accuracy from a series of calibrations, wherein appropriately oriented ruby single crystals were stressed along the respective principal axes and the corresponding piezospectroscopic shifts recorded, with details described in Ref [114].

When Cr-doped Al_2O_3 is strained, the frequency of the Cr^{3+} luminescence shifts from its stress-free value. By assuming a flat alumina scale, the stress is presumed to be in a biaxial compression, i.e., σ_{xx}=σ_{yy}=σ and σ_{zz}=0, therefore, Eq. 5.1 can be reduced to

$$\overline{\Delta\nu} = \frac{2}{3} \prod_{ii} \sigma, \tag{5.2}$$

where the value of the trace of the piezospectroscopic tensor, $\prod_{ii}$ equals to 7.6 cm^{-1}/GPa. Fig. 5.4 shows a typical photoluminescence spectrum of R1'-R2' double (shifted from stress-free R1-R2 due to presence of stress) from α-Al_2O_3 and Q1-Q2 doublet from θ-Al_2O_3 with the dash line marked the frequency position of R2 line in the stress-free state.

5.4 XRD

X-ray diffraction (XRD) provides information about compounds and crystalline phases which presented in materials. In this work, a XPERT-PRO X-ray diffractometer was used to identify the oxides species on oxidized coating surface. The analyses were made in grazing incident mode. Characteristic Cu Kα radiation (λ=1.54178 Å) from a copper anode X-ray tube was used as the radiation source. When sample surface is hit by X-rays at the incident angle θ, the radiation is diffracted at an angle θ from the crystal planes (hkl) if the Bragg law, $2d_{hkl}sin\theta$ =

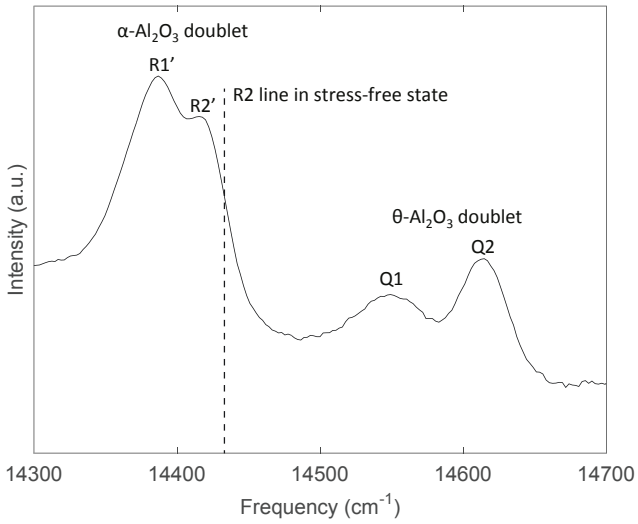

Figure 5.4. Typical photoluminescence spectrum of R1'-R2' double (shifted from stress-free R1-R2 due to presence of stress) from α-Al_2O_3 and Q1-Q2 doublet from θ-Al_2O_3. The dash line indicates the frequency position of R2 line in the stress-free state.[60]

$n\lambda$ (n=1, 2, 3...), is satisfied, where d_{hkl} is the inter-planer spacing, λ the wavelength of radiation and n is order of diffraction [115]. The crystal structure and the phase composition can be identified by retrieving the diffraction angle and the intensity of the diffracted beams. As presented in Fig. 5.5, XRD patterns of oxidized coatings were recorded.

5.5 Thermodynamic modeling

Thermodynamic modeling was performed by using Thermo-Calc software. It is a software for calculation of phase diagrams and thermodynamic properties based on CALPHAD method, which has been developed since 1970s [117]. A powerful feature of the software is the possibility to obtain analytical derivatives of thermodynamic quantities with respect to equilibrium conditions. By using the Ni-based thermodynamic database (latest release: TCNI8), it is possible to calculate the aluminium activity of long-term oxidized MCrAlY coatings for coating lifetime evaluation.

As aforementioned, activity is a measure of the "effective" concentration of a species in the system which can be used to define equilibrium constant [104].

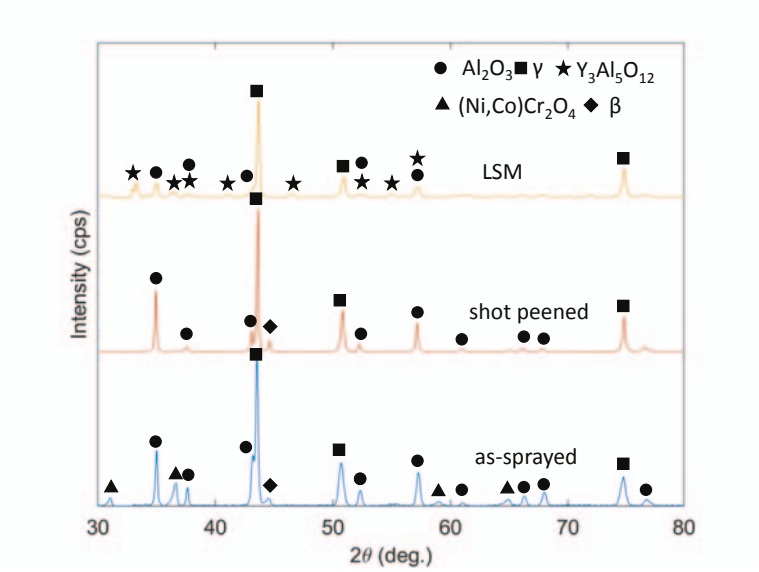

Figure 5.5. XRD patterns recorded on three oxidized coatings [116].

The calculation of element activity in equilibrium is identical to evaluating partial derivatives of total Gibbs energy, ΔG_{total}, with respect to variables at thermodynamic equilibrium as described in Ref. [118]. This is performed by solving Lagrangian multipliers of the equilibrium calculation optimization problem in Thermo-Calc software [104]. And it is worthy to mention that ΔG_{total} is a function of all elements in the system, indicating Al activity calculation in Thermo-Calc software also depends on other elements in the system. The work-flow used in this study is described in Fig. 5.6 [32]:

1. EDS measurement of composition in interested area;
2. Define alloy system with composition obtained from step 1 and temperature as a condition in equilibrium module "POLY";
3. Calculate equilibrium of current system by minimization of ΔG_{total} derived from thermodynamic database using Thermo-Calc software;
4. Calculate Al activity based on the equilibrium from step 3.

For the evaluation of Al activity as a function of oxidation time, the time dependent composition changes are also considered. Fig. 5.7 shows an example on the results

of aluminium activity derived from Thermo-Calc software.

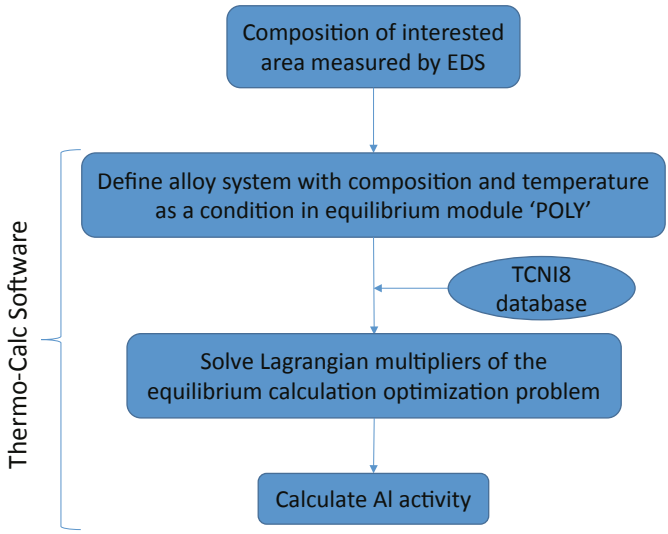

Figure 5.6. Workflow of Al activity calculation method in this study [32].

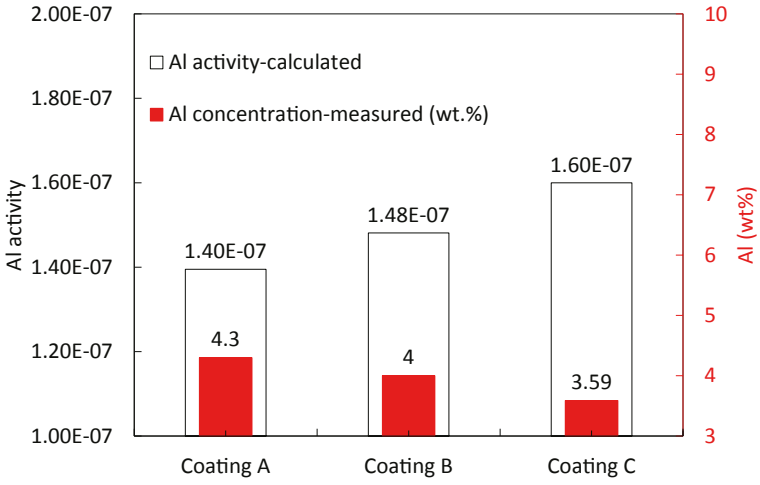

Figure 5.7. Comparison of the Al activity and Al concentration in three MCrAlY coatings. The Al activity is calculated using Thermo-Calc software [32].

5.6 Microscopy

Scanning electron microscope (SEM) was used to analyze the microstructure, morphology and chemical compositions in materials. The SEM used in this thesis work is a SU-70 Hitachi system (Japan). Two modes are commonly used, i.e., secondary electron (SE) mode and back scattered electron (BSE) mode. SE mode was applied to capture the morphology of sample surface due to its high spatial resolution; BSE mode, on the contrary, has a low depth resolution but high contrast to the chemical variation (elemental contrast), and plastic deformation. Microanalysis of chemical compositions was performed in SEM by energy or wavelength dispersive spectroscopes (EDS or WDS). With the interaction between electron beam and samples, characteristic X-rays of corresponding elements can be identified. The quantitative measurement of chemical composition of interested area was performed by EDS with the correction of ZAF parameter from a pure Co standard. Fig. 5.8 gives an example of surface morphology of polished NiCoCrAlY coating after oxidation at 1000 ℃ for various times: alumina oxide morphology features at different magnifications were captured in SE mode, a β+γ two-phase structure was exhibited under BSE mode in Fig. 5.8a.

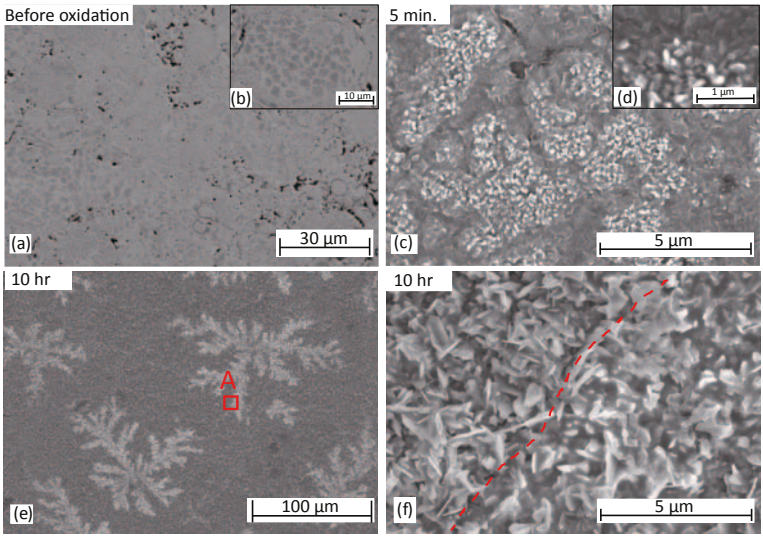

Figure 5.8. Surface morphology of NiCoCrAlY coating after oxidation for various times, with insets showing the localized alumina scale at higher magnification. a, b) BSE image of partially melted powder structure; f) higher magnification of region A in e)[60].

CHAPTER 6

Summary of Appended Papers

Paper I: Long-term oxidation of MCrAlY coatings at 1000 °C and an Al-activity based coating life criterion.

A reliable criterion to estimate the capability of coating to form α-Al_2O_3 is of great importance to accurately evaluate coating lifetime. However, the use of empirical Al-concentration based criterion fails to predict the formation of a continuous α-Al_2O_3 scale in some cases, therefore, a new life criterion, namely the critical Al-activity criterion, is proposed.

Survey of published results on a number of binary Ni-Al and ternary Ni-Cr-Al, Ni-Al-Si systems shows that the empirical Al-concentration based criterion is inadequate to properly predict the formation of a continuous α-Al_2O_3 scale. On the other hand, correlating the corresponding Al-activity data, calculated from measured chemical compositions using the Thermo-Calc software, to the experimental oxidation results has revealed a temperature dependent, critical Al-activity value for forming continuous α-Al_2O_3 scale.

To support the criterion, long-term oxidation tests were performed: five different MCrAlY coatings coated on IN-792 superalloy substrates were oxidized at 1000 °C for various periods of time up to 10,000 h. The new critical Al-activity criterion has been successfully adopted in α-Al_2O_3 formation prediction, showing a good agreement with experiment results. Therefore, it can be concluded that the

extrapolation of new criterion from binary and ternary systems to multi-alloyed MCrAlY system is reasonable. Furthermore, the partial pressure of oxygen (p_{O_2}) in atmosphere has been taken into consideration by combination with Al-activity to calculate the critical chemical reaction constant (K) of formation of α-Al_2O_3. The potential applicability of the methodology to predict MCrAlY life is also discussed. In addition, the results showed complicated interdiffusion behaviour near coating and substrate interface. The inward diffusion of Co and Cr from coating to substrate destabilized γ' in substrate and the outward diffusion of Ti and Ta from substrate to coating stabilized γ' in both substrate and coating.

The criterion developed in this paper could be useful for the prediction of MCrAlY lifetime in industrial application, also provide a tool for MCrAlY coating composition design.

Paper II: A multi-approach study of transient→alpha transformation in alumina scale formed on HVAF-sprayed NiCoCrAlY coatings and the effect of surface treatment.

The aim of this paper is to investigate the transient-to-alpha alumina phase transformation during initial oxidation stage of MCrAlY coatings. The effect of surface treatments, such as mechanical polishing and shot-peening, are also discussed. HVAF sprayed MCrAlY coatings were surface treated after deposition using mechanical polishing and shot-peening process. Three groups of MCrAlY coatings, including: as-sprayed, polished and shot-peened, were oxidized at 1000 ℃ for various time, and the weight gain of oxidized samples were recorded. After oxidation test, the evolution of the scale microstructure, morphology, phase composition, preferential scale nucleation site, residual stress, oxidation kinetics and cross-sectional microstructure were investigated using several experimental techniques, such as scanning electron microscopy (SEM), photo-stimulated luminescence spectroscopy (PSLS), and weight gain method.

The results showed that both polished and shot-peened coatings exhibited superior performance due to rapid formation of α-Al_2O_3 fully covering the coating and suppressing growth of transient alumina, assisted by high density of α-Al_2O_3 nuclei on surface treatment induced defects. Moreover, the early development of a two-layer alumina scale consisting of an inward-grown inner α-Al_2O_3 layer and an outer layer transformed from outward-grown transient alumina resulted in higher oxide growth rate of the as-sprayed coating. Schematic illustrations of phase con-

stitutions, transformation and growth of oxide scale formed on as-sprayed coating, polished coating and shot-peened coating at different oxidation stages are proposed to better describe the influence of surface treatment.

Paper III: Isothermal oxidation behavior of HVAF-sprayed NiCoCrAlY coatings: Effect of surface treatment.

This paper also investigated the surface treatment effects on oxidation of MCrAlY coatings, however, at a longer oxidation time compared with paper II. The effect of surface treatment by means of shot-peening and laser surface melting (LSM) on the oxidation resistance of HVAF-sprayed NiCoCrAlY coatings was studied by performing isothermal oxidation test at 1000 ℃ for 1000 h.

The results showed that shot-peening treatment produced a compact, smooth uniform surface instead of a very rough surface with dispersed un-melted powders as in the as-sprayed coating. The surface roughness of the shot-peened coating was significantly reduced. Spinels and α-Al_2O_3 mixed oxide formed on as-sprayed coating surface were observed, in contrast, a dense protective α-Al_2O_3 layer formed on the shot-peened coating surface without spinels.

The laser surface melting treated coating surface showed a different morphology: smooth melting paths with some bulged nodules in the gap between melting paths and few bugled nodules dispersed on the paths. After the thermal exposure at 1000 ℃ for 1000 h, only α-Al_2O_3 was observed on LSM treated surface and the low growth rate of α-Al_2O_3 oxide was due to the early selective oxidation of Y-rich oxide on the bugled nodules after the LSM treatment.

The results of paper II and III reveal the positive effects of post-deposition surface treatment on improving coating oxidation resistance, which is beneficial for the optimization of coating production process in industry.

CHAPTER 7

Conclusions

The present research focuses on the investigation of the oxidation behavior of MCrAlY coatings at different oxidation stages. The following conclusions offer better understandings of the oxide scale development during oxidation, also provide tools for the coating design and optimization of coating production process in industrial application.

1. Post-deposition surface treatments improve oxidation performance of HVAF-sprayed MCrAlY coatings. A two-layer structure of α-Al_2O_3 scale forms on NiCoCrAlY coatings during oxidation, which consists of an outer layer transformed from outward grown transient alumina and an inward grown inner α-Al_2O_3 layer. Polishing and especially shot-peening treatment suppress the fast growth of transient alumina by improving fast formation of protective inner α-Al_2O_3 scale, resulting in a much thinner outer α-Al_2O_3 layer, i.e. a lower overall oxide scale growth rate compared with as-sprayed state at initial oxidation stage.

2. For longer oxidation times, the positive effect of surface treatments on coating oxidation resistance is significant. Surface treatments, such as shot-peening and laser-surface-melting, aid the formation of compact α-Al_2O_3 suppressing spinels formation and reduce the oxide growth rate, which is

beneficial for coating long-term oxidation performance.

3. An Al-activity based coating life criterion is developed, successfully adopted in α-Al_2O_3 formation prediction of MCrAlY coatings.

4. Complicated interdiffusion behaviour near coating and substrate interface occurs during oxidation. After long-term oxidation, the inward diffusion of Co and Cr from coating to substrate destabilized γ' in substrate and the outward diffusion of Ti and Ta from substrate to coating stabilized γ' in both substrate and coating.

Bibliography

[1] *SGT-750 industrial gas turbine*. URL: https://www.siemens.com/global/en/home/products/energy.html.

[2] *SGT-750 industrial gas turbine*. URL: https://en.wikipedia.org/wiki/Fossil_fuel_power_station.

[3] R.C. Reed. *The superalloys: fundamentals and applications*. Cambridge University Press, 2008.

[4] J.R. Davis et al. *ASM specialty handbook: heat-resistant materials*. Asm International, 1997.

[5] J.R. Nicholls. *Advances in Coating Design for High-Performance Gas Turbines*. Vol. 28. 09. Cambridge University Press, 2003, pp. 659–670.

[6] M.P. Boyce. *Gas Turbine Engineering Handbook*. 2006, p. 956.

[7] *SGT-750 industrial gas turbine*. URL: https://www.siemens.com/global/en/home/products/energy/power-generation/gas-turbines/sgt-750.html#!/.

[8] C. G. Levi. "Emerging materials and processes for thermal barrier systems". In: *Current Opinion in Solid State and Materials Science* 8.1 (2004), pp. 77–91.

[9] G.Y. Lai. *High-temperature corrosion and materials applications*. ASM International, 2007.

[10] Y. Tamarin. *Protective coatings for turbine blades*. ASM international, 2002.

[11] R.A. Cottis et al. *Shreir's corrosion*. Elsevier Amsterdam, 2010.

[12] K. Yuan. "Oxidation and Corrosion of New MCrAlX Coatings : Modelling and Experiments". PhD thesis. Linköping University, Engineering Materials, 2014, p. 27.

[13] J.R. Nicholls, N.J. Simms, W.Y. Chan, and H.E. Evans. "Smart overlay coatings-concept and practice". In: *Surface and Coatings Technology* 149.2 (2002), pp. 236–244.

[14] R. Sivakumar and B.L. Mordike. "High temperature coatings for gas turbine blades: a review". In: *Surface and Coatings Technology* 37.2 (1989), pp. 139–160.

[15] S. Bose. *High temperature coatings*. Butterworth-Heinemann, 2011.

[16] J.G. Smeggil. "Some comments on the role of yttrium in protective oxide scale adherence". In: *Materials Science and Engineering* 87 (1987), pp. 261–265.

[17] H.J. Grabke. "Oxidation of NiAl and FeAl". In: *Intermetallics* 7.10 (1999), pp. 1153–1158.

[18] J. Foster, B.P. Cameron, and J.A. Carew. "The production of multi-component alloy coatings by particle codeposition". In: *Transactions of the IMF* 63.1 (1985), pp. 115–119.

[19] W.J. Quadakkers, V. Shemet, D. Sebold, R. Anton, E. Wessel, and L. Singheiser. "Oxidation characteristics of a platinized MCrAlY bond coat for TBC systems during cyclic oxidation at 1000 ℃". In: *Surface and Coatings Technology* 199.1 (2005), pp. 77–82.

[20] N. Czech, F. Schmitz, and W. Stamm. "Improvement of MCrAlY coatings by addition of rhenium". In: *Surface and Coatings Technology* 68 (1994), pp. 17–21.

[21] F. Juarez, D. Monceau, D. Tetard, B. Pieraggi, and C. Vahlas. "Chemical vapor deposition of ruthenium on NiCoCrAlYTa powders followed by thermal oxidation of the sintered coupons". In: *Surface and Coatings Technology* 163 (2003), pp. 44–49.

[22] H.E. Evans and M.P. Taylor. "Diffusion Cells and Chemical Failure of MCrAlY Bond Coats in Thermal-Barrier Coating Systems". In: *Oxidation of Metals* 55.1 (2001), pp. 17–34.

[23] J.A. Haynes, B.A. Pint, W.D. Porter, and I.G. Wright. "Comparison of thermal expansion and oxidation behavior of various high-temperature coating materials and superalloys". In: *Materials at High Temperatures* 21.2 (2004), pp. 87–94.

[24] D. Stöver and C. Funke. "Directions of the development of thermal barrier coatings in energy applications". In: *Journal of Materials Processing Technology* 92 (1999), pp. 195–202.

[25] B. Gudmundsson and B.E. Jacobson. "Yttrium oxides in vacuum-plasma-sprayed CoNiCrAlY coatings". In: *Thin Solid Films* 173.1 (1989), pp. 99–107.

[26] N.P. Padture, M. Gell, and E.H. Jordan. "Thermal barrier coatings for gas-turbine engine applications". In: *Science* 296.5566 (2002), pp. 280–284.

[27] M. Gell, L. Xie, X. Ma, E.H. Jordan, and N.P. Padture. "Highly durable thermal barrier coatings made by the solution precursor plasma spray process". In: *Surface and Coatings Technology* 177 (2004), pp. 97–102.

[28] D. Toma, W. Brandl, and U. Köster. "Studies on the transient stage of oxidation of VPS and HVOF sprayed MCrAlY coatings". In: *Surface and Coatings Technology* 120 (1999), pp. 8–15.

[29] W. Brandl, D. Toma, J. Krüger, H.J. Grabke, and G. Matthäus. "The oxidation behaviour of HVOF thermal-sprayed MCrAlY coatings". In: *Surface and Coatings Technology* 94 (1997), pp. 21–26.

[30] D. Strauss, G. Müller, G. Schumacher, V. Engelko, W. Stamm, D. Clemens, and W.J. Quaddakers. "Oxide scale growth on MCrAlY bond coatings after pulsed electron beam treatment and deposition of EBPVD-TBC". In: *Surface and Coatings Technology* 135.2 (2001), pp. 196–201.

[31] B.M. Warnes. "Improved aluminide/MCrAlX coating systems for super alloys using CVD low activity aluminizing". In: *Surface and Coatings Technology* 163 (2003), pp. 106–111.

[32] P. Zhang, K. Yuan, R. Lin Peng, X.-H. Li, and S. Johansson. "Long-term oxidation of MCrAlY coatings at 1000 °C and an Al-activity based coating life criterion". In: *Surface and Coatings Technology* 332 (2017), pp. 12–21.

[33] J.X. Yang, Q. Zheng, H.Y Zhang, X.F. Sun, H.R. Guan, and Z.Q. Hu. "Effects of heat treatments on the microstructure of IN792 alloy". In: *Materials Science and Engineering: A* 527.4 (2010), pp. 1016–1021.

[34] S. Saeidi, K.T. Voisey, and D.G. McCartney. "The effect of heat treatment on the oxidation behavior of HVOF and VPS CoNiCrAlY coatings". In: *Journal of Thermal Spray Technology* 18.2 (2009), pp. 209–216.

[35] J.T. DeMasi-Marcin and D.K. Gupta. "Protective coatings in the gas turbine engine". In: *Surface and Coatings Technology* 68 (1994), pp. 1–9.

[36] M. Gell, J. Eric, V. Krishnakumar, K. McCarron, B. Barber, Y.H. Sohn, and V.K. Tolpygo. "Bond strength, bond stress and spallation mechanisms of thermal barrier coatings". In: *Surface and Coatings Technology* 120 (1999), pp. 53–60.

[37] B.A. Pint, I.G. Wright, W.Y. Lee, Y. Zhang, K. Pruessner, and K.B. Alexander. "Substrate and bond coat compositions: factors affecting alumina scale adhesion". In: *Materials Science and Engineering: A* 245.2 (1998), pp. 201–211.

[38] E.P. Busso, J. Lin, S. Sakurai, and M. Nakayama. "A mechanistic study of oxidation-induced degradation in a plasma-sprayed thermal barrier coating system.: Part I: model formulation". In: *Acta Materialia* 49.9 (2001), pp. 1515–1528.

[39] W.R. Chen, X. Wu, B.R. Marple, and P.C. Patnaik. "The growth and influence of thermally grown oxide in a thermal barrier coating". In: *Surface and Coatings Technology* 201.3 (2006), pp. 1074–1079.

[40] W.R. Chen, X. Wu, B.R. Marple, and P.C. Patnaik. "Oxidation and crack nucleation/growth in an air-plasma-sprayed thermal barrier coating with NiCrAlY bond coat". In: *Surface and Coatings Technology* 197.1 (2005), pp. 109–115.

[41] R. Eriksson, M. Gupta, E. Broitman, K.P. Jonnalagadda, P. Nylén, and R. Peng. "Stresses and cracking during chromia-spinel-NiO cluster formation in TBC systems". In: *Journal of Thermal Spray Technology* 24.6 (2015), pp. 1002–1014.

[42] H. Hindam and D.P. Whittle. "Microstructure, adhesion and growth kinetics of protective scales on metals and alloys". In: *Oxidation of Metals* 18.5 (1982), pp. 245–284.

[43] I. Barin, O. Knacke, and O. Kubaschewski. *Thermochemical properties of inorganic substances*. Springer, 1977, p. 861.

[44] N. Eliaz, G. Shemesh, and R.M. Latanision. "Hot corrosion in gas turbine components". In: *Engineering Failure Analysis* 9.1 (2002), pp. 31–43.

[45] R.A. Rapp. "Hot corrosion of materials: a fluxing mechanism?" In: *Corrosion Science* 44.2 (2002), pp. 209–221.

[46] I. Gurrappa. "Hot corrosion of protective coatings". In: *Materials and Manufacturing Processes* 15.5 (2000), pp. 761–773.

[47] J.R. Nicholls. "Designing oxidation-resistant coatings". In: *Journal of Metals* 52.1 (2000), p. 28.

[48] S. Kamal, R. Jayaganthan, and S. Prakash. "Hot corrosion studies of detonation-gun-sprayed NiCrAlY+ 0.4 wt.% CeO_2 coated superalloys in molten salt environment". In: *Journal of materials engineering and performance* 20.6 (2011), pp. 1068–1077.

[49] S. Krämer, J. Yang, C.G. Levi, and C.A. Johnson. "Thermochemical interaction of thermal barrier coatings with molten CaO–MgO–Al_2O_3–SiO_2 (CMAS) deposits". In: *Journal of the American Ceramic Society* 89.10 (2006), pp. 3167–3175.

[50] J.A. Goebel and F.S. Pettit. "Na_2SO_4-induced accelerated oxidation (hot corrosion) of nickel". In: *Metallurgical and Materials Transactions B* 1.7 (1970), pp. 1943–1954.

[51] J.A. Goebel, F.S. Pettit, and G.W. Goward. "Mechanisms for the hot corrosion of nickel-base alloys". In: *Metallurgical and Materials Transactions B* 4.1 (1973), pp. 261–278.

[52] R.A. Rapp. "Chemistry and electrochemistry of hot corrosion of metals". In: *Materials Science and Engineering* 87 (1987), pp. 319–327.

[53] R.C. Reed, T. Tao, and N. Warnken. "Alloys-by-design: application to nickel-based single crystal superalloys". In: *Acta Materialia* 57.19 (2009), pp. 5898–5913.

[54] P. Kofstad. "High temperature corrosion". In: *Elsevier Applied Science Publishers* (1988).

[55] N. Birks, G.H. Meier, and F.S. Pettit. *Introduction to the high temperature oxidation of metals*. Cambridge University Press, 2006, pp. 39–74.

[56] A.S. Khanna. *Introduction to high temperature oxidation and corrosion*. ASM international, 2002.

[57] A.G. Evans, D.R. Clarke, and C.G. Levi. "The influence of oxides on the performance of advanced gas turbines". In: *Journal of the European Ceramic Society* 28.7 (2008), pp. 1405–1419.

[58] D.A. Jones. *Principles and prevention of corrosion*. Macmillan, 1992.

[59] D.M. Lipkin, H. Schaffer, F. Adar, and D.R. Clarke. "Lateral growth kinetics of α-alumina accompanying the formation of a protective scale on (111) NiAl during oxidation at 1100 ℃". In: *Applied Physics Letters* 70.19 (1997), pp. 2550–2552.

[60] P. Zhang, E. Sadeghimeresht, S. Chen, X.-H. Li, N. Markocsan, S. Joshi, W. Chen, I.A. Buyanova, and R. Lin Peng. *A multi-approach study of transient-to-alpha transformation in alumina scale formed on HVAF-sprayed NiCoCrAlY coating and the effect of surface treatment*. submitted to Corrossion Science, 2018.

[61] M.W. Brumm and H.J. Grabke. "The oxidation behaviour of NiAl-I. Phase transformations in the alumina scale during oxidation of NiAl and NiAl-Cr alloys". In: *Corrosion Science* 33.11 (1992), pp. 1677–1690.

[62] P.T. Moseley, K.R. Hyde, B.A. Bellamy, and G. Tappin. "The microstructure of the scale formed during the high temperature oxidation of a Fecralloy steel". In: *Corrosion science* 24.6 (1984), pp. 547–565.

[63] A.L. Dragoo and J.J. Diamond. "Transitions in Vapor-Deposited Alumina from 300° to 1200° C". In: *Journal of the American Ceramic Society* 50.11 (1967), pp. 568–574.

[64] K.M.N. Prasanna, A.S. Khanna, R. Chandra, and W.J. Quadakkers. "Effect of θ-alumina formation on the growth kinetics of alumina-forming superalloys". In: *Oxidation of Metals* 46.5-6 (1996), pp. 465–480.

[65] H. Svensson. "Initial Oxidation of β-NiAl(Pt) Coatings and Model Alloys". PhD thesis. 2006.

[66] W.G. Sloof and T.J. Nijdam. "On the high-temperature oxidation of MCrAlY coatings". In: *International Journal of Materials Research* 100.10 (2009), pp. 1318–1330.

[67] F.H. Stott, G.C. Wood, and J. Stringer. "The influence of alloying elements on the development and maintenance of protective scales". In: *Oxidation of Metals* 44.1-2 (1995), pp. 113–145.

[68] D. Toma, W. Brandl, and U. Köster. "The characteristics of alumina scales formed on HVOF-sprayed MCrAlY coatings". In: *Oxidation of Metals* 53.1 (2000), pp. 125–137.

[69] T.J. Nijdam, L.P.H. Jeurgens, J.H. Chen, and W.G. Sloof. "On the microstructure of the initial oxide grown by controlled annealing and oxidation on a NiCoCrAlY bond coating". In: *Oxidation of Metals* 64.5-6 (2005), pp. 355–377.

[70] J.L. Smialek. "Effect of sulfur removal on Al_2O_3 scale adhesion". In: *Metallurgical Transactions A* 22.3 (1991), pp. 739–752.

[71] J.L. Smialek and B.K. Tubbs. "Effect of sulfur removal on scale adhesion to PWA 1480". In: *Metallurgical and Materials Transactions A* 26.2 (1995), pp. 427–435.

[72] J.L. Smialek, D.T. Jayne, J.C. Schaeffer, and W.H. Murphy. "Effects of hydrogen annealing, sulfur segregation and diffusion on the cyclic oxidation resistance of superalloys: a review". In: *Thin Solid Films* 253.1-2 (1994), pp. 285–292.

[73] K. Yuan, R. Lin Peng, X.-H. Li, S. Johansson, and Y.-D. Wang. "Some aspects of elemental behaviour in HVOF MCrAlY coatings in high-temperature oxidation". In: *Surface and Coatings Technology* 261 (2015), pp. 86–101.

[74] R. Mévrel. "State of the art on high-temperature corrosion-resistant coatings". In: *Materials Science and Engineering: A* 120 (1989), pp. 13–24.

[75] M.P. Brady, B.A. Pint, P.F. Tortorelli, I.G. Wright, and R.J. Hanrahan. "High-Temperature Oxidation and Corrosion of Intermetallics". In: *Materials Science and Technology* (2000).

[76] R. Prescott, D.F. Mitchell, M.J. Graham, and J. Doychak. "Oxidation mechanisms of β-NiAl+ Zr determined by SIMS". In: *Corrosion Science* 37.9 (1995), pp. 1341–1364.

[77] A. Strawbridge and P.Y. Hou. "The role of reactive elements in oxide scale adhesion". In: *Materials at high temperatures* 12.2-3 (1994), pp. 177–181.

[78] B.A. Pint. “The role of chemical composition on the oxidation performance of aluminide coatings”. In: *Surface and Coatings Technology* 188 (2004), pp. 71–78.

[79] B.A. Pint. “Experimental observations in support of the dynamic-segregation theory to explain the reactive-element effect”. In: *Oxidation of Metals* 45.1 (1996), pp. 1–37.

[80] P.Y. Hou and K. Priimak. “Interfacial segregation, pore formation, and scale adhesion on NiAl alloys”. In: *Oxidation of Metals* 63.1 (2005), pp. 113–130.

[81] P. Burtin, J.P. Brunelle, M. Pijolat, and M. Soustelle. “Influence of surface area and additives on the thermal stability of transition alumina catalyst supports. I: Kinetic data”. In: *Applied Catalysis* 34 (1987), pp. 225–238.

[82] Y. Niu, X.J. Zhang, Y. Wu, and F. Gesmundo. “The third-element effect in the oxidation of Ni–xCr–7Al (x= 0, 5, 10, 15 at.%) alloys in 1 atm O_2 at 900–1000 °C”. In: *Corrosion science* 48.12 (2006), pp. 4020–4036.

[83] D. Renusch, B. Veal, K. Natesan, and M. Grimsditch. “Transient oxidation in Fe-Cr-Ni alloys: A Raman-scattering study”. In: *Oxidation of Metals* 46.5 (1996), pp. 365–381.

[84] J. He, Z. Zhang, H. Peng, S. Gong, and H. Guo. “The role of Dy and Hf doping on oxidation behavior of two-phase ($\gamma'+\beta$) Ni–Al alloys”. In: *Corrosion Science* 98 (2015), pp. 699–707.

[85] S. Salam, P.Y. Hou, Y.D. Zhang, H.F. Wang, C. Zhang, and Z.G. Yang. “Compositional effects on the high-temperature oxidation lifetime of MCrAlY type coating alloys”. In: *Corrosion Science* 95 (2015), pp. 143–151.

[86] G. Pulci, J. Tirillò, F. Marra, F. Sarasini, A. Bellucci, T. Valente, and C. Bartuli. “High temperature oxidation and microstructural evolution of modified MCrAlY coatings”. In: *Metallurgical and Materials Transactions A* 45.3 (2014), pp. 1401–1408.

[87] P. Zhang, R. Lin Peng, X.-H. Li, and Johansson S. “Influence of Ce and Ru on the Behaviour of HVOF NiCoCrAlX Coatings in High Temperature Oxidation”. In: *Proceedings of International Thermal Sprayed Conference (ITSC)* (2016), pp. 635–640.

[88] W. Qi, H. Peng, J. He, S. Li, S. Gong, and H. Guo. "Cyclic oxidation and interdiffusion behavior of Pt modified NiAlHfCrSi coatings on single crystal superalloy containing Mo". In: *Surface and Coatings Technology* 259 (2014), pp. 426–433.

[89] S.M. Jiang, H.Q. Li, J. Ma, C.Z. Xu, J. Gong, and C. Sun. "High temperature corrosion behaviour of a gradient NiCoCrAlYSi coating II: oxidation and hot corrosion". In: *Corrosion Science* 52.7 (2010), pp. 2316–2322.

[90] J. Shi, H.Q. Li, MQ. Wan, H.L. Wang, and X. Wang. "High temperature oxidation and inter-diffusion behavior of electroplated Ni–Re diffusion barriers between NiCoCrAlY coating and orthorhombic-Ti_2AlNb alloy". In: *Corrosion Science* 102 (2016), pp. 200–208.

[91] H. Guo, Y. Cui, H. Peng, and S. Gong. "Improved cyclic oxidation resistance of electron beam physical vapor deposited nano-oxide dispersed β-NiAl coatings for Hf-containing superalloy". In: *Corrosion Science* 52.4 (2010), pp. 1440–1446.

[92] W. Brandl, G. Marginean, D. Maghet, and D. Utu. "Effects of specimen treatment and surface preparation on the isothermal oxidation behaviour of the HVOF-sprayed MCrAlY coatings". In: *Surface and Coatings Technology* 188 (2004), pp. 20–26.

[93] A.C. Karaoglanli, K.M. Doleker, B. Demirel, A. Turk, and R. Varol. "Effect of shot peening on the oxidation behavior of thermal barrier coatings". In: *Applied Surface Science* 354 (2015), pp. 314–322.

[94] K.M. Doleker and A.C. Karaoglanli. "Comparison of oxidation behavior of shot-peened plasma spray coatings with cold gas dynamic spray coatings". In: *Oxidation of Metals* 88.1-2 (2017), pp. 121–132.

[95] J. Cai, P. Lv, Q. Guan, X. Xu, J. Lu, Z. Wang, and Z. Han. "Thermal cycling behavior of thermal barrier coatings with MCrAlY bond coat irradiated by high-current pulsed electron beam". In: *ACS applied materials & interfaces* 8.47 (2016), pp. 32541–32556.

[96] J. Cizek, M. Matejkova, J. Kouril, J. Cupera, and I. Dlouhy. "Potential of New-Generation Electron Beam Technology in Interface Modification of Cold and HVOF Sprayed MCrAlY Bond Coats". In: *Advances in Materials Science and Engineering* 2016 (2016).

[97] G. Marginean and D. Utu. “Cyclic oxidation behaviour of different treated CoNiCrAlY coatings”. In: *Applied Surface Science* 258.20 (2012), pp. 8307–8311.

[98] J. Cai, S.Z. Yang, L. Ji, Q.F. Guan, Z.P. Wang, and Z.Y. Han. “Surface microstructure and high temperature oxidation resistance of thermal sprayed CoCrAlY coating irradiated by high current pulsed electron beam”. In: *Surface and Coatings Technology* 251 (2014), pp. 217–225.

[99] J.C. Pereira, J.C. Zambrano, M.J. Tobar, A. Yañez, and V. Amigó. “High temperature oxidation behavior of laser cladding MCrAlY coatings on austenitic stainless steel”. In: *Surface and Coatings Technology* 270 (2015), pp. 243–248.

[100] V. Teleginski, D.C. Chagas, A.C.C. de Oliveira, J.G. Santos, J.F. Azevedo, R. Riva, and G. de Vasconcelos. “Yb: fiber laser surface texturing of stainless steel substrate, with MCrAlY deposition and CO_2 laser treatment”. In: *Surface and Coatings Technology* 260 (2014), pp. 251–259.

[101] G. Pulci, J. Tirillò, F. Marra, F. Sarasini, A. Bellucci, T. Valente, and C. Bartuli. “High temperature oxidation of MCrAlY coatings modified by Al_2O_3 PVD overlay”. In: *Surface and Coatings Technology* 268 (2015), pp. 198–204.

[102] Y. Li, C. Li, Q. Zhang, L. Xing, and G. Yang. “Effect of chemical compositions and surface morphologies of MCrAlY coating on its isothermal oxidation behavior”. In: *Journal of Thermal Spray Technology* 20.1-2 (2011), pp. 121–131.

[103] B. Rajasekaran, G. Mauer, and R. Vaßen. “Enhanced characteristics of HVOF-sprayed MCrAlY bond coats for TBC applications”. In: *Journal of Thermal Spray Technology* 20.6 (2011), pp. 1209–1216.

[104] E.R. Cohen. *Quantities, units and symbols in physical chemistry*. Royal Society of Chemistry, 2007.

[105] J.T. Yardley. *Introduction to Molecular Energy Transfer*. Academic Press, 1980, p. 308.

[106] D.W. Marquardt. “An algorithm for least-squares estimation of nonlinear parameters”. In: *Journal of the society for Industrial and Applied Mathematics* 11.2 (1963), pp. 431–441.

[107] H.G. Drickamer. "The effect of high pressure on the electronic structure of solids". In: *Solid State Physics* 17 (1965), pp. 1–133.

[108] D.S. McClure. "Electronic Spectra of Molecules and Ions in Crystals. Part II. Spectra of Ions in Crystals". In: *Solid State Physics* 9 (1959), pp. 399–525.

[109] B. Henderson and G.F. Imbusch. *Optical spectroscopy of inorganic solids*. Vol. 44. Oxford University Press, 2006.

[110] Q.Z. Wen, D.M. Lipkin, and D.R. Clarke. "Luminescence Characterization of Chromium-Containing theta-Alumina". In: *Journal of the American Ceramic Society* 81.12 (1998), pp. 3345–3348.

[111] A. Reddy, D.B. Hovis, A.H. Heuer, A.P. Paulikas, and B.W. Veal. "In situ study of oxidation-induced growth strains in a model NiCrAlY bond-coat alloy". In: *Oxidation of Metals* 67.3-4 (2007), pp. 153–177.

[112] J. He and D.R. Clarke. "Determination of the Piezospectroscopic Coefficients for Chromium-Doped Sapphire". In: *Journal of the American Ceramic Society* 78.5 (1995), pp. 1347–1353.

[113] L. Grabner. "Spectroscopic technique for the measurement of residual stress in sintered Al_2O_3". In: *Journal of Applied Physics* 49.2 (1978), pp. 580–583.

[114] D.M. Lipkin, and D.R. Clarke. "Measurement of the stress in oxide scales formed by oxidation of alumina-forming alloys". In: *Oxidation of Metals* 45.3 (1996), pp. 267–280.

[115] V.K. Pecharsky and P.Y. Zavalij. *Fundamentals of powder diffraction and structural characterization of materials*. Vol. 69. Springer, 2009.

[116] P. Zhang, E. Sadeghimeresht, R. Lin Peng, X.-H. Li, N. Markocsan, and S. Joshi. "Isothermal oxidation behavior of HVAF-sprayed NiCoCrAlY coatings : Effect of surface treatment". In: *Proceedings of International Thermal Sprayed Conference (ITSC)* (2017), pp. 456–461.

[117] J. Andersson, T. Helander, L. Höglund, P. Shi, and B. Sundman. "Thermo-Calc & DICTRA, computational tools for materials science". In: *Calphad* 26.2 (2002), pp. 273–312.

[118] H. Larsson and M. Jansson. "Rate of change at equilibrium". In: *Calphad* 51.Supplement C (2015), pp. 220 –223.

Papers

The papers associated with this thesis have been removed for copyright reasons. For more details about these see:

http://urn.kb.se/resolve?urn=urn:nbn:se:liu:diva-145095